ELSEVIER

Contents lists available at ScienceDirect

Journal of Colloid and Interface Science

journal homepage: www.elsevier.com/locate/jcis



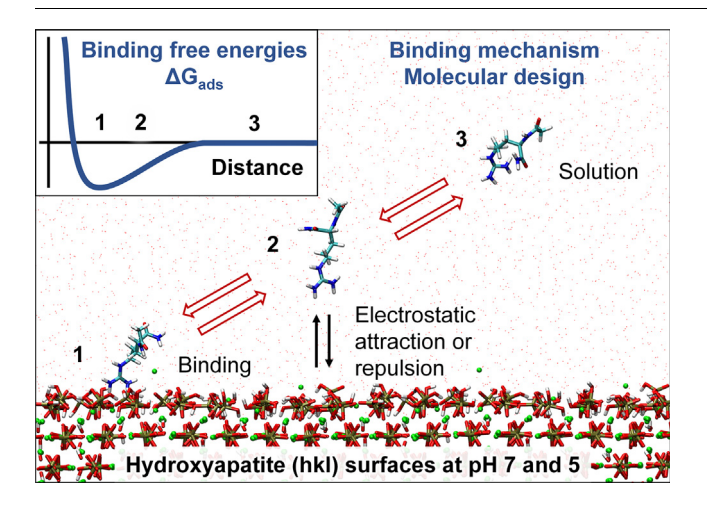
Binding mechanism and binding free energy of amino acids and citrate to hydroxyapatite surfaces as a function of crystallographic facet, pH, and electrolytes



Samuel E. Hoff^a, Juan Liu^{a,b}, Hendrik Heinz^{a,*}

- ^a Department of Chemical and Biological Engineering, University of Colorado Boulder, Boulder, CO 80309, USA
- ^b Department of Materials Science and Engineering, Dalian Maritime University, Dalian, Liaoning 116026, China

G R A P H I C A L A B S T R A C T



ARTICLE INFO

Article history: Received 27 March 2021 Revised 19 July 2021 Accepted 20 July 2021 Available online 23 July 2021

ABSTRACT

Hydroxyapatite (HAP) is the major mineral phase in bone and teeth. The interaction of individual amino acids and citrate ions with different crystallographic HAP surfaces has remained uncertain for decades, creating a knowledge gap to rationally design interactions with peptides, proteins, and drugs. In this contribution, we quantify the binding mechanisms and binding free energies of the 20 end-capped natural amino acids and citrate ions on the basal (001) and prismatic (010)/(020) planes of hydroxyapatite at pH values of 7 and 5 for the first time at the molecular scale. We utilized over 1500 steered molecular dynamics simulations with highly accurate potentials that reproduce surface and hydration energies of (hkl) hydroxyapatite surfaces at different pH values. Charged residues demonstrate a much higher affinity to HAP than charge-neutral species due to the formation of superficial ion pairs and ease of penetration into layers of water molecules on the mineral surface. Binding free energies range from 0 to -60 kJ/mol and were determined with $\sim 10\%$ uncertainty. The highest affinity was found for citrate, followed by Asp (-) and Glu(-), and followed after a gap by Arg(+), Lys(+), as well as by His(+) at pH 5. The (hkl)-specific area density of calcium ions, the protonation state of phosphate ions, and subsurface directional order of the ions in HAP lead to surface-specific binding patterns. Amino acids without ionic side groups exhibit weak binding, between -3 and 0 kJ/mol, due to difficulties to penetrate the first layer of water molecules

E-mail address: hendrik.heinz@colorado.edu (H. Heinz).

^{*} Corresponding author.

on the apatite surfaces. We explain recognition processes that remained elusive in experiments, in prior simulations, discuss agreement with available data, and reconcile conflicting interpretations. The findings can serve as useful input for the design of peptides, proteins, and drug molecules for the modification of bone and teeth-related materials, as well as control of apatite mineralization.

© 2021 Elsevier Inc. All rights reserved.

1. Introduction

Bone and teeth are hierarchically structured composite materials that form in biomineralization reactions under physiological conditions. The mineral phase primarily consists of hydroxyapatite (HAP), $Ca_{10}(PO_4)_6(OH)_2$, a polymorph of calcium phosphate-hydroxide, and is embedded in type I collagen [1], as well as various non-collagenous proteins (NCPs) and citrate. Many attempts have been made to mimic the natural biomineralization process, for example, using peptide sequences, to varying degrees of success [2–5]. Proteins, peptides, as well as other species such as citric acid [6,7] are known to promote, direct, or inhibit hydroxyapatite nucleation and growth depending on composition and solution conditions [8–15].

A common method to identify bone mineral-binding peptides is phage display [2]. Several amino acid sequences with notable binding and mineralization activity have been identified, however, progress in uncovering new sequences and interpreting functionality is slow. For example, limiting the peptide length to 15 amino acids, the pool of potential peptide sequences for binding to HAP is already in the quintillions. To-date, the operating mechanisms at the molecular scale remain uncertain and it has been impossible to filter out which peptides would function best. Fundamental understanding of the interactions at the molecular level is required to move towards rational methods to test and design peptide sequences for bone regeneration and drug delivery, or to modify proteins such as osteocalcin and statherin for specific functions [16–18]. The current resolution of microscopy techniques for such interfaces is about 100 times too low, at \sim 1 nm, to examine such interfaces. It is extremely challenging to localize organic molecules on HAP surfaces, and when measurements are feasible, the data are typically averages over a collection of surface features and large numbers of molecules.

Within these limits, several experimental studies provide valuable insights into the binding affinities of amino acids to hydroxyapatite [14,19–22]. The techniques include, for example, transmission electron microscopy (TEM), scanning electron microscopy (SEM), nuclear magnetic resonance (NMR) [22], atomic force microscopy (AFM) [23], as well as X-ray diffraction (XRD), colorimetric methods, X-ray photoelectron spectroscopy, and vibrational spectroscopy [19,23,24]. Charged amino acids were suggested to have the strongest affinity towards HAP; however, conflicting data exist whether positively or negatively charged amino acids are preferred, and the order of magnitude is uncertain [21,25,26]. Gonzalez-McQuire et al. suggest that the binding affinity increases in the order of apolar < positively charged < polar < negatively charged [27], placing polar amino acids in the vicinity of charged amino acids. Jahromi et al. reported stronger adsorption of positively charged Arg than negatively charged Glu [19]. Overall, the significance of electrostatic interactions for binding to hydroxyapatite surfaces has been pointed out, which is consistent with established amino acid binding mechanisms to other charged mineral surfaces such as silica and clay minerals [28,29]. At the same time, it is difficult to distinguish (hkl) crystal facets and monitor the binding process in-situ. Essential changes in surface chemistry were often disregarded as they are elusive to microscopy due to the current resolution limits. Studies with peptides were typically carried out at pH ~ 7 and have not covered lower pH values of ~ 5

relevant for bone fracture and healing sites [30]. As medical treatment is important at low pH sites, acidic environments are critical to study. In summary, there is a range of observations that needs to be explained while the binding mechanisms, the order of the binding affinity of various amino acids, the role of (*hkl*) facets, pH values, electrolytes, and quantitative free energies are still unknown.

To answer some of the open questions, in silico studies such as molecular dynamics (MD) simulations have been employed to investigate binding mechanisms and affinities of peptides and amino acids to HAP facets [31-35]. However, computational studies prior to using the Interface Force Field (IFF) [36-38] have two very significant problems, namely, unrealistic simulation conditions and incomplete validation of the force fields. First, unmodified HAP crystal surfaces such as (010) and (001) have been used prior to IFF, causing misleading results [22,23,31-34,39]. Unmodified (hkl) surfaces of HAP are only stable at pH values > 14 and do not occur in living systems which feature pH values in a typical range between 3 and 10. Under physiological conditions, the neat HAP surfaces undergo hydration, protonation, and reconstruction, which involves the dissolution and protonation of superficial hydroxide ions, changes in the protonation state of superficial phosphate species, and reductions in the area density of superficial calcium ions between 40% and 70% (Fig. 1) [36]. Therefore, studies on surfaces corresponding to pH > 14 have little practical value. Second, earlier force field parameters for HAP [40] have been missing a chemical rationale, assume misleading atomic charges in excess of 100%, and include no validation of cleavage and hydration energies relative to experimental data [24,36,41-47], which would be important for reliability and compatibility with biomolecular force fields. As a result of these drawbacks in prior simulations of apatite and phosphate-related systems, previously computed binding conformations of amino acids, peptides, and proteins are misleading. In one study, interaction energies up to -2000 kJ/mol (-500 kcal/mol) per functional group were reported [48], which are difficult to relate to experiments as they assume pH > 14 and exclude the contribution of solvent and electrolytes [14,49]. Recent MD and DFT simulations of the adsorption of phosphorylated Ser and Glu on HAP (001) and (100) surfaces at pH > 14 report binding free energies on the same order of our reported values (0 to -60 kJ/mol), however, interpretations remain difficult due to the chosen pH value and force field [35]. Quantum methods such as density functional theory (DFT) could be an alternative, however, DFT calculations do not capture the needed length scale and electrolyte dynamics, and face challenges to accurately predict surface binding at the nanoscale [50,51].

In this work, we overcome these limitations. We analyze, quantify, and explain the interactions of amino acids and citrate with hydroxyapatite surfaces at atomic resolution, including facet-specific differences and physiologically relevant pH values, using cutting-edge MD simulations (Fig. 1). Precise understanding of interactions of single amino acids with HAP is a necessary first step to quantify molecular driving forces involved in the recognition and assembly of bone-related materials. We utilize MD simulations with the Interface Force Field (IFF), which represents the chemical bonding well and includes physically justified atomic charges [52], includes an interpretation of all parameters, is consistent with parameters for other inorganic and organic compounds, and underwent rigorous validation [36]. Thereby, IFF overcomes the

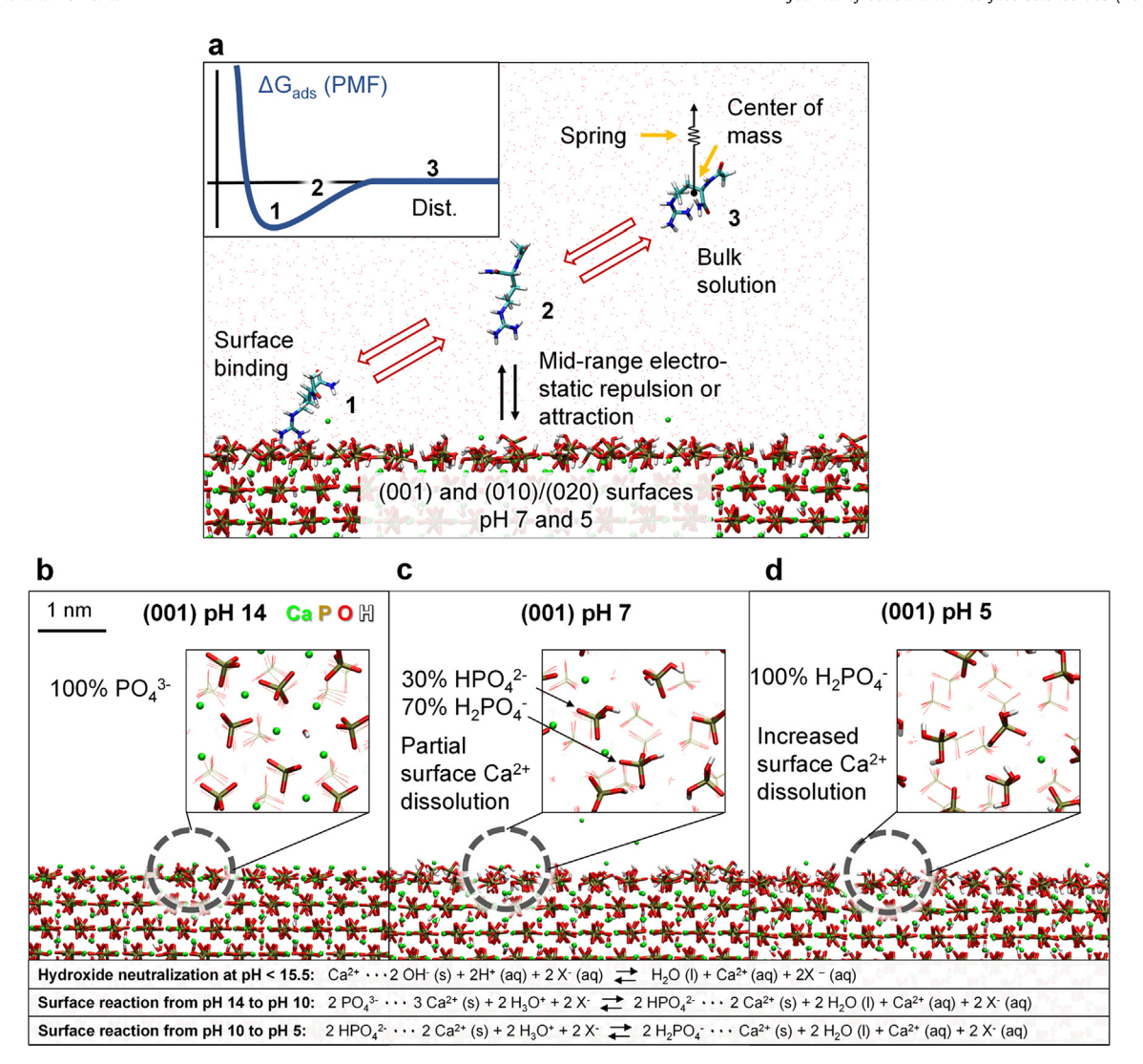


Fig. 1. Analysis of amino acid binding to hydroxyapatite (HAP) surfaces, $Ca_{10}(PO_4)_6(OH)_2$, and important details of the HAP surface chemistry. (a) Schematic to determine the free energy profile of amino acid binding as a function of distance using steered molecular dynamics simulations (also called potential of mean force, PMF). The inset in the top left represents the schematic free energy profile. The main panel shows the amino acid Arg bound to the HAP surface (1), detachment or association with the surface, respectively (2), and desorption out of the range of interaction in bulk solution (3). (b-d) Views of the (001) HAP surface at various pH values. At a pH = 14, neutralization of hydroxide ions (pK ~ 15.7) occurs and reduces the Ca^{2+} density relative to cleavage planes in vacuum. The side view at pH = 14 with an inset of the top view shows 100% of phosphate ions (PO $_4^3$) on the surface and a high area density of calcium ions (b). Continued protonation to pH = 7 leads to a mixture of 30% HPO $_4^3$ ions and 70% H2PO $_4$, resulting in less than half the surface charge compared to pH 14 (c). At pH = 5, the surface consists of 100% H2PO $_4$ ions, with 30% less calcium ions present per surface area than at pH 7 (d). The acid-base reactions on the surface are summarized at the bottom and likewise occur on other (hkl) surfaces such as (010)/(020) (see Ref. [36]).

abovementioned limitations of earlier force fields. Specifically, it reproduces the crystal structure of HAP within ± 0.5%, the (hkl) surface energies, pH dependence, and hydration energies known from experiments within approximately ± 10%, and is compatible with biomolecular force fields [36,37]. Recent MD simulations using IFF-CHARMM36 explained the formation of amorphous calcium phosphate prenucleation clusters and interactions with collagen in agreement with experiments [53]. Binding energies and free energies of peptides and amino acids on chemically similar, pHresponsive silica surfaces [54] and other nanostructures have been computed with<10% deviation from experimental reference data [55–62]. Here, we employed the IFF models for hydroxyapatite surfaces in contact with aqueous solution at pH values of 7 and 5. Surface chemistry and protonation states are consistent with pK values of phosphoric acid and data from infrared spectroscopy as documented in the IFF surface model database (Fig. 1) [36]. Interestingly, the cation densities and Ca/P ratios on HAP surfaces at pH = 7 are less than half in comparison to pH = 14, and the calcium ions exhibit statistical surface disorder at all pH value lower than 14 [24,36]. Models for pH 7 and pH 5 environments were therefore created by modifications of the surface chemistry using specific ratios of H₂PO₄ ions to HPO₂²⁻ ions, determined by the pK values (acidity constants) of phosphoric acid, available spectroscopic data from experiments, as well as maintaining the stoichiometry of the associated reactions and overall charge neutrality (Fig. 1b-d) [36].

We then analyzed the binding of 20 natural single amino acids and citrate ions using models of (010)/(020) and (001) HAP surfaces at pH values of 7 and 5 (Fig. 1a). Methods included steered molecular dynamics (SMD) and unrestrained molecular dynamics (MD) simulation in all-atom detail using IFF-CHARMM36 parameters, including the CHARMM36 parameters for the organic molecules, and extensive sampling of over 1500 adsorption-desorption curves. The simulation protocol involved slow, reversible pulling of the molecules towards and away from the surfaces (Fig. 1a). Hereby, (010) and (020) surfaces transition into one another under aqueous conditions and we used the (020) surface

of lower energy. Hydroxyapatite surfaces were represented at different pH values by neutralizing hydroxide ions, adjusting the protonation state of the surface phosphate layer, and the amount of calcium ions for charge neutrality (Fig. 1b-d) [36]. Adjustments in surface chemistry under *in vitro* and *in vivo* conditions occur via buffer solutions, which regulate the area density of ions, protonated phosphate species, and interfacial assembly. All amino acids were acylated at the *N*-terminal and amidated at the C-terminal to identify the role of side groups (Fig. 1). Alternative models of the amino acids in the zwitterionic state were not chosen as they might not accurately reflect the contribution of side groups to surface adsorption [33,63]. Citric acid was included due to the known high concentration in bone tissue and *in vivo* importance [64].

2. Results and discussion

In this section, we describe the binding free energies of the capped amino acids, the binding mechanism and origin of binding differences, the role of the HAP (*hkl*) surface structure, interactions at medium range, water layering at the interfaces, as well as the affinity as a function of the local surface environment. We discuss the influence of pH value, salinity, and temperature, interpret available experimental data, and explain future opportunities.

2.1. Binding free energies

The free energies of adsorption ΔG of all 20 amino acids and citrate (Cit) were obtained on the (001) and (020) surfaces at pH values of 5 and 7 from over 1500 SMD and unrestrained MD simulations (Fig. 2). The two surfaces form the common basal and prismatic planes of hydroxyapatite crystals, respectively. The affinity of the amino acids decreases in the order negatively charged > positively charged ≥ uncharged in a range from -40 kJ/mol to 0 kJ/mol, while citrate with up to 3 ionic groups adsorbs with a strength up to $-60 \, \text{kJ/mol}$. The results are of high precision with <±3 kI/mol statistical deviation. The accuracy is expected in a similar range (<±10%) due to prior validation of IFF for HAP-water interfacial interactions, for which experimental reference data are available [24,36,41-44], and the demonstrated reliability of IFF for chemically similar inorganic-organic systems [37,65-67]. Our study is the first quantitative analysis of the affinity of all amino acids and citrate to HAP to-date, including specific crystal facets and physiological pH values. Earlier results are only available for selected amino acids with high uncertainty, including unlikely surface chemistries at pH > 14 in prior simulations [22,34,35].

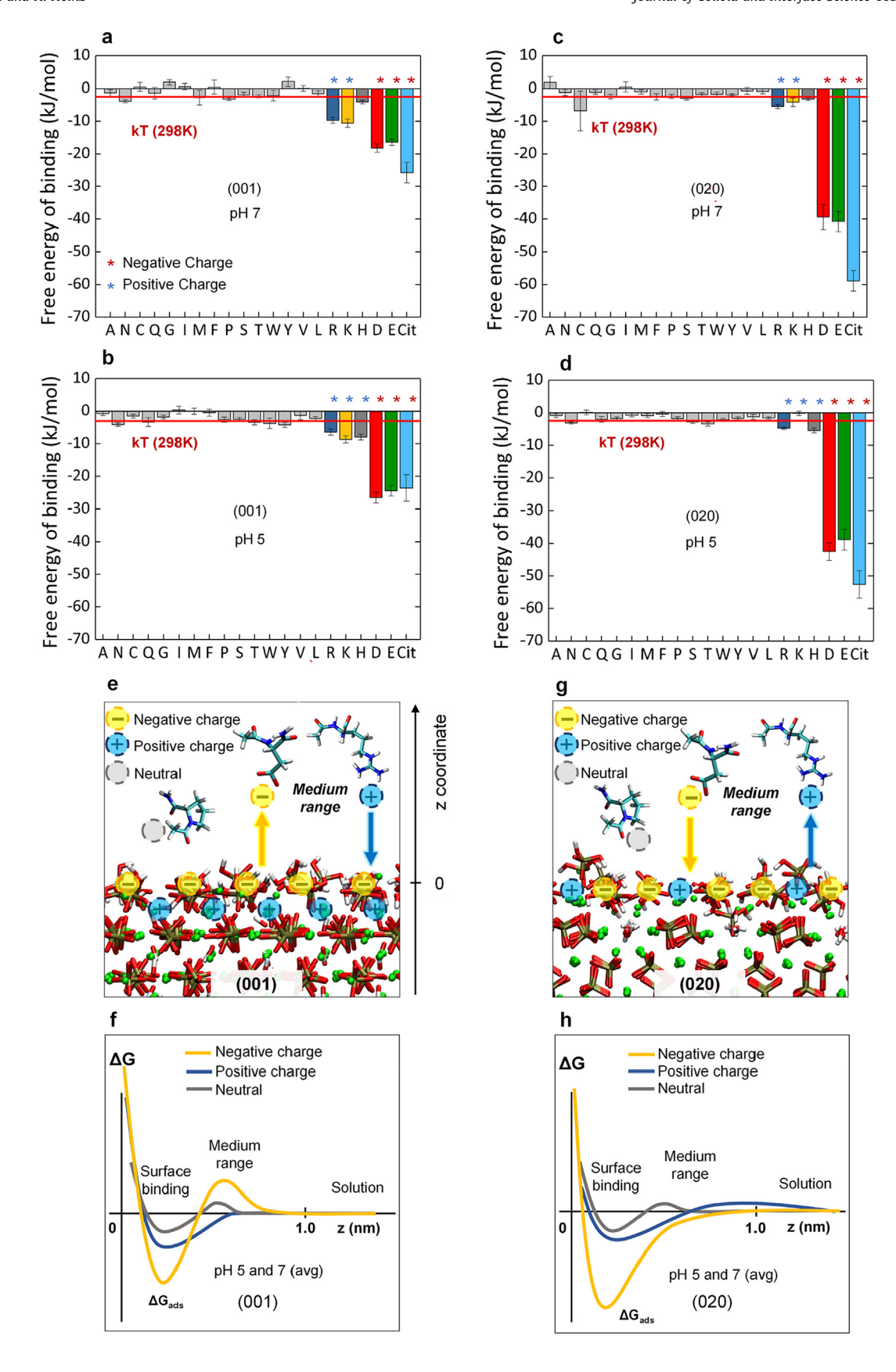
On the basal (001) plane, the negatively charged amino acids D (-) and E(-) exhibit the largest adsorption free energies (Fig. 2a, b). The values amount to -18 and -27 kJ/mol for D(-) at pH 7 and 5, respectively, and -16 and -25 kJ/mol for E(-) at pH 7 and 5, respectively. The affinities for D and E are the same within the uncertainty and related to the formation of local ion pairs between carboxylate groups and calcium ions on the HAP surface. The mechanism is clearly seen in the analysis of the trajectories and will be discussed further below (Movies S1 and S2, Figure S1 in the Supporting Material, and Large Dataset of trajectories). Citrate is attracted by -26 and -24 kJ/mol at pH 7 and 5, respectively, whereby the citrate charge is -3 at pH 7 and reduced to -2 at pH 5 due to partial protonation (consistent with pK values of 3.1, 4.7, and 6.4) [68]. Significant adsorption was also seen for R(+) at -11 and -8 kJ/mol at pH values of 7 and 5, respectively, and for K(+) at -12 and -10 kJ/mol at pH 7 and 5, respectively. Furthermore, H(0) adsorbs with -5 kJ/mol at pH 7 and H(+) with -9 kJ/mol at pH 5, respectively (Fig. 2a, b). Hereby, H changes the protonation state from (near-)neutral at pH 7 to positively charged at pH 5 and then adsorbs almost twice as strong compared to pH 7.

The remaining amino acids have comparatively weak adsorption. N displays weak attraction of -4 kJ/mol at pH 5 and at pH 7. T, W, and Y show some attraction on the order of -3 to -4 kJ/mol at pH 5. The binding strength tends to be less than -3 kJ/mol for A, C, Q, G, I, M, F, P, S, T, W, Y, V, and L at pH 7 and at pH 5 (Fig. 2a, b). Overall, neutral residues have difficulties to penetrate the closest water layers atop the ionic HAP surface, cannot form ion pairs, and van-der-Waals interactions lead to minimal adsorption (Movie S1 in the Supplementary Material). A breakdown of electrostatic and van-der-Waals contributions to adsorption for the charged molecules shows that changes in electrostatic interactions, namely, ion pairing, account for the large share of attraction (Figure S2 in the Supporting Material). Hydrogen bonds and van-der-Waals interactions preexist before adsorption, only rearrange after adsorption, and therefore make a small or negligible contribution to the binding free energy (Figure S3 in the Supporting Material). These observations are consistent with earlier findings for peptide and polymer adsorption on similarly charged silica and calcium silicate hydrate surfaces [28,29,57,58], and we elaborate on mechanistic details in later sections below.

The trends in binding free energies of amino acids are similar for the prismatic (020) surface, which due to precipitationdissolution equilibria is a more realistic representation of the (010) surface (Fig. 2c, d) [36]. The negatively charged molecules D and E both adsorb strongly with approximately -40 ± 3 kJ/mol at pH 5 and 7, showing little differentiation with respect to pH and side group, which differs only by a methylene unit. Binding of D(-) is characterized by -39 ± 4 and -43 ± 3 kJ/mol at pH 7 and 5, respectively, and E(-) adsorbs with -41 ± 3 and -38 ± 3 kJ/mol at pH 7 and 5, respectively. Citrate is the strongest binder at -58 ± 4 and -52 ± 5 kJ/mol, respectively, for a charge of -3 at pH = 7 and a charge of -2 at pH = 5, respectively (Fig. 2c, d). Binding is relatively unaffected by the pH value. The free energy of adsorption of the negatively charged amino acids D, E, and citrate on the prismatic (020) plane is almost twice as strong as on the basal (001) plane (Fig. 2c, d), which is related to the surface chemistry as explained in the sections further below. The binding free energy of R(+) is -6 and -5 kJ/mol at pH values of 7 and 5, respectively, and adsorption of K(+) is -4 and 0 kJ/mol at pH values of 7 and 5, respectively. This attraction is much weaker than on the (001) surface. In particular, K(+) is only marginally or not at all attracted to the (020) surface (Fig. 2c, d). Adsorption of H(0) amounts to -4 kJ/mol and of H(+) to -6 kJ/mol at pH 7 and 5, respectively, somewhat reduced compared to the basal (001) plane. The positive charge at pH 5 slightly improves adsorption of H(+). Weak attraction of -4 kJ/mol is observed for N and T at pH 5. The non-ionic amino acids A, N, C, Q, G, I, M, F, P, S, T, W, Y, V, and L typically exhibit a binding strength less than -3 kJ/mol at pH 7 and at pH 5 on the (020) surface (Fig. 2c, d).

2.2. Binding Mechanism, origin of binding Differences, and role of the HAP surface structure

The calculated free energies of binding illustrate that only charged species exhibit significant attraction ($\gg 1~kT = 2.4~kJ/mol$) to the (001) and (020) surfaces at the two chosen pH values. The origin of significant binding lies nearly exclusively in ion pairing, which varies depending on the (hkl) HAP surface and the associated layered structure of ionic groups (Fig. 2e-h, Movies S1 and S2). Van-der-Waals interactions only rearrange without significant gains or losses and contribute marginally to binding (Figure S2 in the Supporting Material). Hydrogen bonds, which have an approximate strength of 18–20 kJ/mol in water (=difference of vaporization energy of water of 40.7 kJ/mol [68] minus van-der-Waals contributions, divided by two hydrogen bonds per molecule), do not contribute to binding in a significant way as they pre-exist



between amino acids and water, between water molecules, as well as between hydrogen phosphate surfaces and water, and only rearrange upon binding. In support, we found no change in the average total number of hydrogen bonds before and after adsorption for two amino acid-HAP pairs, Glu and Lys on (001) HAP surfaces at pH 7 as examples, monitoring over the entire simulation time (Figure S3 in the Supporting Material). Small contributions to binding are possible from changes in the geometry and in the strength of individual hydrogen bonds. All amino acids display some affinity towards the HAP surface, likely related to ion-dipole interactions of polar groups, including capping end groups, with the ions on the mineral surface. The contribution of capping end groups likely increases binding affinities of all amino acids by a uniform small amount. Since side chains of non-charged amino acids generally showed little to no attraction to HAP due to competition with surface-bound water, the focus of our remaining discussion will be on the charged residues.

Examination of the free energy profiles as a function of distance shows differences in short-range interactions (<0.3 nm) and medium-range (<1.2 nm) interactions with HAP, which are largely dictated by the surface structure (Fig. 2e-h). The high density of calcium ions and protonated phosphate species on the surface of HAP cause a larger negative binding free energy of negatively charged and positively charged amino acids versus neutral amino acids at close distance, i.e., <0.3 nm from the nearest surface atom. These short-range interactions are determined by the local chemical composition of the HAP surface. The charge profile of the specific (hkl) HAP surface further determines mid-range interactions between 0.3 nm and 1.2 nm from the nearest surface atom. Specifically, the (001) surface contains a layered structure of protonated phosphate ions at the top, followed by a layer of calcium and hydroxide ions beneath (Fig. 2e). Therefore, it features a layer of negative charge of protonated phosphate ions followed by a layer of positive charge of calcium ions. Incoming charged molecules see the (001) surface as a negatively charged substrate, leading to favorable interactions with cationic amino acids and slightly unfavorable interactions with anionic amino acids at medium range of 0.3 to 1.2 nm (Fig. 2f). The (020) surfaces (representative of (010) surfaces) feature a more even charge distribution at the mineral-liquid interface, with rows of protonated phosphate ions and calcium ions at the HAP-water interfacial plane that alternate and are parallel to each other (Fig. 2g). This charge distribution is less negative than on the (001) surface, resulting in stronger interactions with anionic amino acids and decreased interactions with cationic amino acids (Fig. 2h). The (020) surface also imposes small energy barriers for cationic amino acids at medium range.

The free energy curves as a function of distance summarize relative trends between groups of amino acids semi-quantitatively (Fig. 2f, h). The amino acids were grouped together based on similarity in binding free energy and dynamics of their approach to the surface.

2.3. Molecule interactions with HAP surfaces from long to medium range

Interactions of amino acids and citrate with the HAP surface are essentially negligible beyond 2 nm distance and remain minimal as the distance decreases to 1.2 nm, given overall charge-neutral surfaces (Fig. 2f, h). The presence of hydroxyapatite surfaces begins to be felt at mid-range distances between 1.2 nm and 0.3 nm when some preferential orientations were observed during the SMD simulations (Fig. 3). The side groups of different amino acids then assumed characteristic orientations relative to the surface (Fig. 3a, b). Thereby, the exact distances that introduce orientation bias depend on the amino acid and on the HAP surface. The (001) surface of hydroxyapatite induced positively charged side groups to be oriented towards the surface and negatively charged side groups to be oriented away (Fig. 3a, b). The (020) surface exhibits an opposite trend, attracting negatively charged side groups, and displaying an overall weaker orientation bias. The trends in orientation bias of the side groups reflect the free energy landscape of the amino acids at medium distance from the surface (12 Å to 3 Å away from the nearest HAP surface atom) and differ from the binding free energy upon direct contact with the surface. A prediction of a favorable versus an unfavorable approach of the amino acids can be made using the charge profile of the solid surface (Fig. 3b-d). Hereby, side group orientation towards the surface indicates favorable association due to opposite charges and vice versa. Most such orientation interactions are residual at 12 Å to 6 Å distance and become stronger within a range of 6 Å to 3 Å from the surface. At distances closer than 3 Å, equilibrium binding between the amino acid and the HAP surface occurs.

The origin of the mid-range interactions with hydroxyapatite surfaces lies in the layered arrangement of ions in the solid phase (Fig. 2e-h and Fig. 3c, d). Density profiles of calcium ions and protonated phosphate ions on the (001) and (020) surfaces at pH 7 illustrate the facet-specific charge profiles (Fig. 3c, d and Figure S4 in the Supporting Material for pH 5). Hereby, z = 0 Å corresponds to the mineral surface, characterized by the average position of P atoms in the top molecular layer of HAP in contact with water (Fig. 3c, d). Negative z coordinates refer to the solid HAP phase and positive z coordinates to the solution phase. Accordingly, the (001) HAP surface is phosphate-rich as it features more protonated phosphate (+25%) and less calcium ions (-50%) in the top molecular layer in comparison to the (020) surface (Fig. 3c). Vice versa, the (020) HAP surface is calcium-rich and exposes comparatively less phosphate species (Fig. 3d). These differences in the structure of (001) and (020) surfaces are also seen in the top view of the outermost molecular layers (Fig. 3e, f). While overall charge-neutral, differences in the specific sequence of layers of ions and associated charge profiles for each (hkl) hydroxyapatite surface explain specific medium-range interactions with charged species, as well as related trends in the equilibrium binding free energies at short range.

Fig. 2. Binding affinity of amino acids and sodium citrate to the (001) and (020) surfaces of hydroxyapatite at pH values of 7 and 5 at 298 K in water. No electrolytes were added except for single Na* and Cl⁻ ions if needed to compensate the charge on ionic groups (\sim 20 mM per added ion). (a, b) Free energy of binding to the (001) surface at pH values of 7 and 5. (c, d) Free energy of binding to the (020) surface at pH values of 7 and 5. Binding affinities much greater than kT(2.5 kJ/mol) are only observed for charged amino acids. (e, f) Charge distribution on the (001) surface and representative free energy profiles of amino acid side group binding as a function of distance. The top atomic layer is dominated by negatively charged protonated phosphate ions, leading to a repulsive barrier for negatively charged groups at a medium distance and attraction of positively charged groups. Among neutral, negatively, and positively charged amino acids, a preference towards negatively charged groups prevails at close distance related to sub-surface and sparce surface calcium ions, along with significant attraction of positively charged groups. (g, h) Charge distribution on the (020) surface and representative free energy profiles of amino acid side group binding as a function of distance. The top atomic layer contains positively charged calcium ions and protonated phosphate species side-by-side, leading to light repulsion (a shallow free energy barrier) for positively charged residues and attraction of negatively charged residues at medium distance of 0.3 to 1.2 nm. Among neutral, negatively charged and positively charged amino acids, a strong preference for negatively charged groups and a weak preference for positively charged groups are seen at close distance < 0.3 nm. For the free energy profiles in (f) and (h), a similar curve shape was observed for pH 5 and 7 that is shown as a qualitative average.

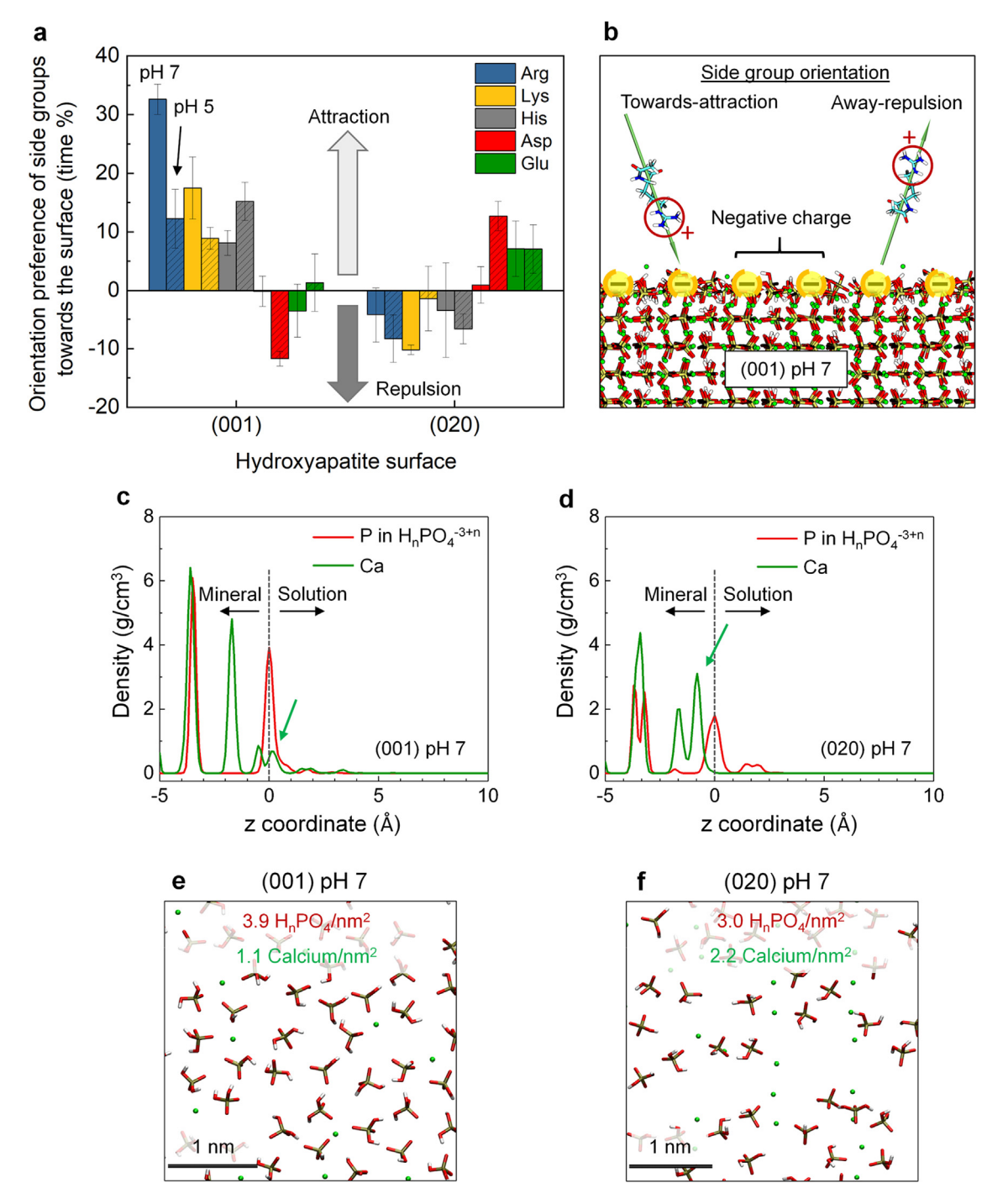


Fig. 3. Dynamic orientation of side chains upon approach to the hydroxyapatite surface and underlying surface geometry controls. (a) Bias in orientation of the amino acid side groups relative to the surface upon approach from the solution from 12 Å to 3 Å distance. The percentage values are relative to 50% of time, e.g., +20% means that the side chain was 70% of time oriented towards the surface and 30% of time oriented away from the surface during steered MD. (b) Example orientations of the arginine (R) side group away from and towards the HAP (001) surface. (c, d) Density profiles of Ca^{2+} ions and P atoms in superficial phosphate species on the (001) and (020) surfaces. The z coordinate was set to 0 Å at the first protonated phosphate layer. The green arrows indicate much lower Ca^{2+} density on the (001) surface than on the (020) surface. As a result, more attraction of R(+) and K(+) side chains, which carry a positive charge, is seen to the (001) surface, and repulsion from the (020) surface. (e, f) Visualization of calcium ions, hydrogenphosphate and dihydrogenphosphate ions in the first layer of the (001) and (020) surfaces of HAP. The different balance between negatively charged and positively charged ions can be visually seen, and results in preferred attraction of side groups with opposite charge as shown in (a).

2.4. Water layering at the interfaces and its barrier function

Solvent molecules on the hydroxyapatite surfaces create an additional barrier in the short-range that the amino acids must overcome for adsorption to occur. The pattern of water distribution, density profile, and penetration into the HAP surface show a strong dependence on the (*hkl*) surface (Fig. 4). The uniform distri-

bution of protonated phosphate species on the (001) surface creates favorable conditions for water association, which can be seen in the form of tightly bound pockets of water approximately 3 Å and 2 Å above the plane of the first phosphate layer (Fig. 4a, b). The (020) facet, in contrast, contains relatively large areas where phosphate species are desorbed into solution (Fig. 4c, d). Combined with an overall lower density of protonated phosphate

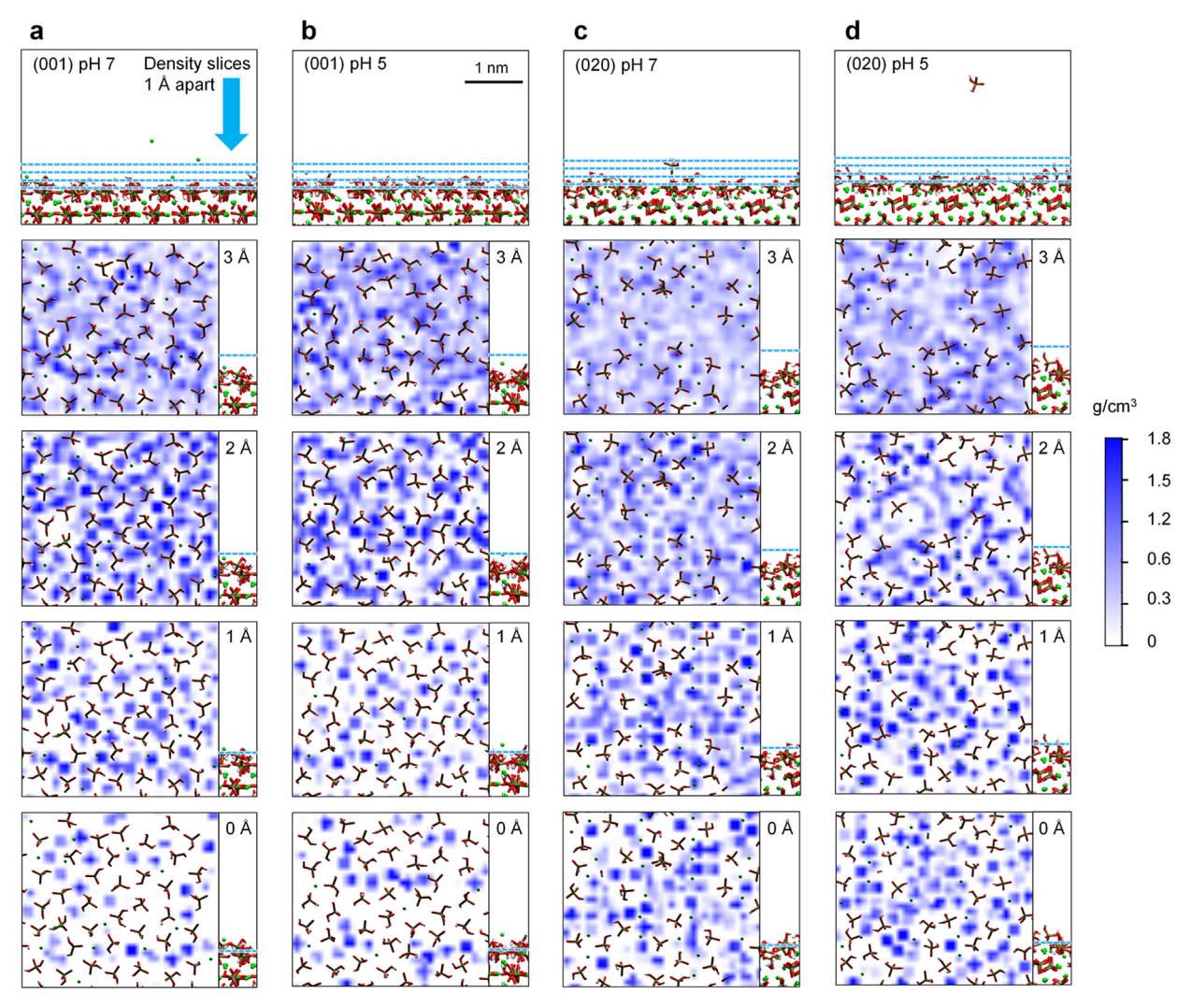


Fig. 4. Water density maps parallel to the hydroxyapatite (001) and (020) surfaces. Every column of panels contains a top panel with side view and the corresponding water density maps in the 4 images below in top view. The blue dotted lines in the top panel in every column indicate the distance of lateral cross sections at 3, 2, 1, and 0 Å from the first phosphate layer. The cross-sectional heights z are given relative to the respective surface plane of phosphorus atoms. Only the first surface layer of calcium and protonated phosphate ions is shown for visual clarity. (a, b) Side view of the (001) surface and lateral water density maps at pH values of 7 and pH 5, respectively. Significant water ordering is seen at 2 and 3 Å distance. The water density is reduced closer to the surface (1 Å), and low water penetration into the first layer of (001) hydroxyapatite (0 Å) is observed. More cavitation is observed at pH 5 compared to pH 7. (c, d) Side view of the (020) surface and lateral water density maps at pH values of 7 and 5, respectively. The (020) surface shows relatively little water densification above the first phosphate layer (2 and 3 Å) due to lower area density of phosphate species and uneven morphology. Solvation of calcium ions in the gap regions of the phosphate species leads to a relatively high local water concentration at 1 and 0 Å and some ordering into vertical columns. Water cavitation is stronger at pH 5 compared to pH 7.

ions, less water densification is observed along with a weak organization into vertical columns. The less dense phosphate layer on the (020) facet supports penetration of water deeper into the HAP surface, seen by internal pockets of water at 1 Å and 0 Å distance (Fig. 4c, d). On the (001) surface, clearly less water penetration is seen past the first phosphate layer (Fig. 4a, b at 1 Å and 0 Å distance). Water penetration into the surface, especially on the (020) surface, suggests that the second layer of phosphate, and further sublayers may also be protonated. A lower pH value of 5 tends to amplify cavitation of the surface relative to pH 7 (Fig. 4b, d), which is noted especially closer to the surface at 0 Å distance and more significant on the (020) surface (Fig. 4d).

While the density maps of water highlight differences among the major (001) and (020) hydroxyapatite surfaces, water layering on both surfaces acts as a barrier and reduces the binding of uncharged amino acids to the HAP surface (Fig. 2). Unrestrained molecular dynamics simulations reveal an inability of the electroneutral amino acids to remove and replace water molecules

bound to the HAP surfaces for over 95% of the simulation time. For example, a video of threonine approaching the HAP surface shows repeated repulsion at the water layer above the surface (Movie S1 in the Supplementary Material). The barriers due to water layering on HAP surfaces and the lack of charge to overcome them lead to small binding free energies of uncharged amino acids on the (001) and (020) HAP surfaces (Fig. 2). Water layering also causes an energy penalty for charged species to interact with the surfaces, however, the barrier is then small compared to the gain in energy upon contact with the HAP surfaces by ion pairing.

2.5. Binding Mechanism, Affinity, and relation to local surface environment

We have thus illustrated that the local surface environment determines the mechanism and extent of binding (Fig. 5). Next, we compare the mechanisms and free energies of binding of the charged amino acids and citrate side-by-side for the hydroxyap-

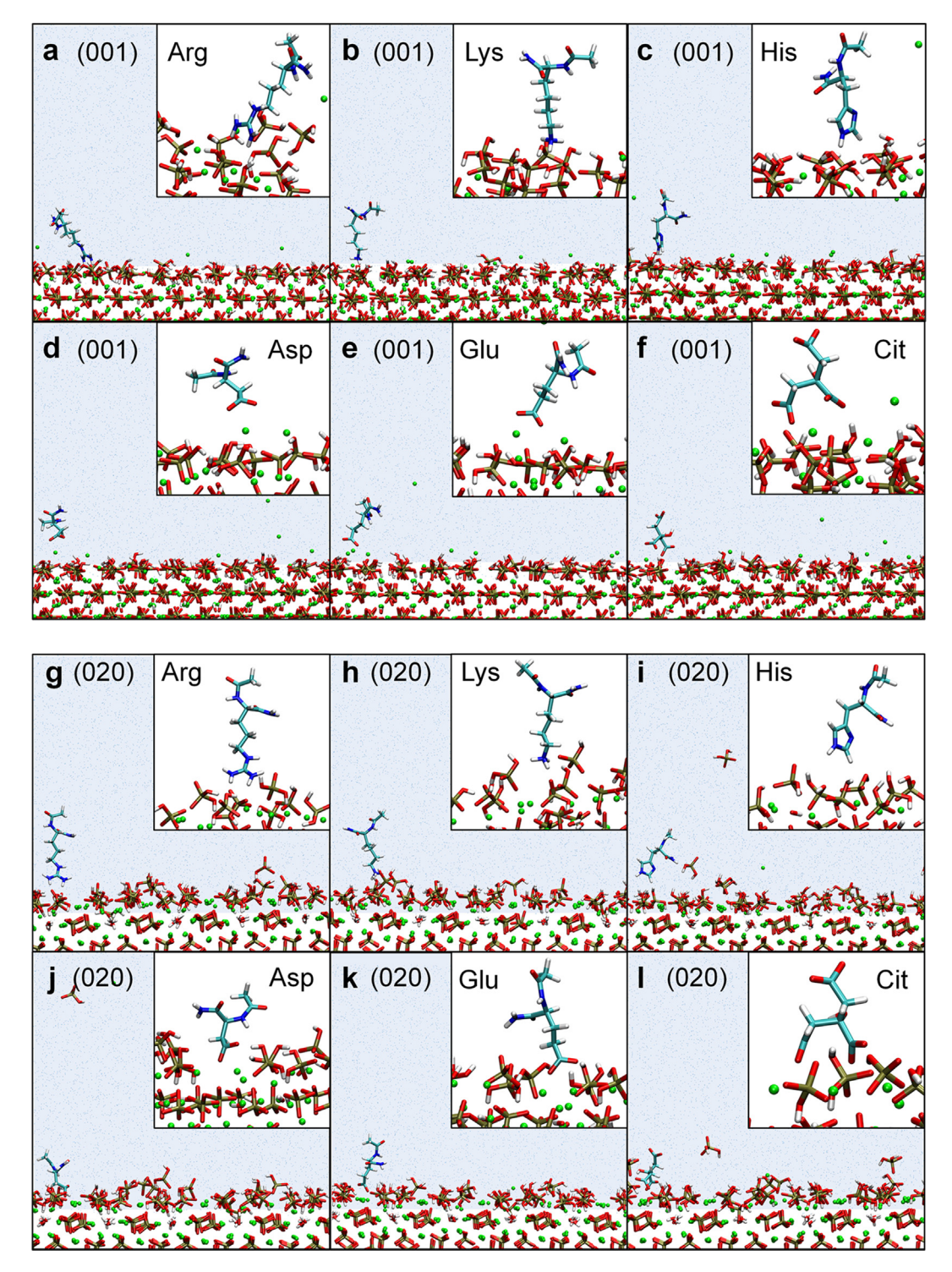


Fig. 5. Representative snapshots of binding conformations of charged amino acids and citrate ions on the hydroxyapatite surfaces at pH 7. The conformations were chosen from steered MD simulations at a distance closely corresponding to the minimum free energy. Counter ions for charge neutrality were Na⁺ or Cl⁻, respectively. (a-f) Charged molecules in contact with (001) surfaces. (g-l) Charged molecules in contact with (020) surfaces. Positively charged amino acids (R, K, H) bind through ion pairing of medium strength and exhibit hydrogen bonding to protonated phosphate species on the surface. Negatively charged amino acids (D, E) and citrate bind through the carboxylate groups to calcium ions exposed on the hydroxyapatite surface via more localized, stronger ion pairing.

atite (001) and (020) surfaces in solutions with pH values of 7 and 5 (Fig. 6). The discussion is supported by visualizations of the simulation trajectories (see Movies S1 and S2 and Large Dataset of trajectories).

Positively charged species (R, K) are attracted via ion pairing of the guanidinium or ammonium groups with surface phosphate species (Fig. 5a, b, g, h). Protonated H(+) binds in a similar fashion at pH 5 (not shown). The positive charge in R and K side groups is distributed over 5 or 3 hydrogen atoms, respectively, and the negative charge is distributed over 2 or 3 oxygen atoms on the protonated phosphate ions, creating delocalized ion pairs, which limit the binding free energy (Fig. 6a). Guanidinium and ammonium groups therefore bind in-between phosphate species and form weak ions pairs with multiple phosphate species. In addition,

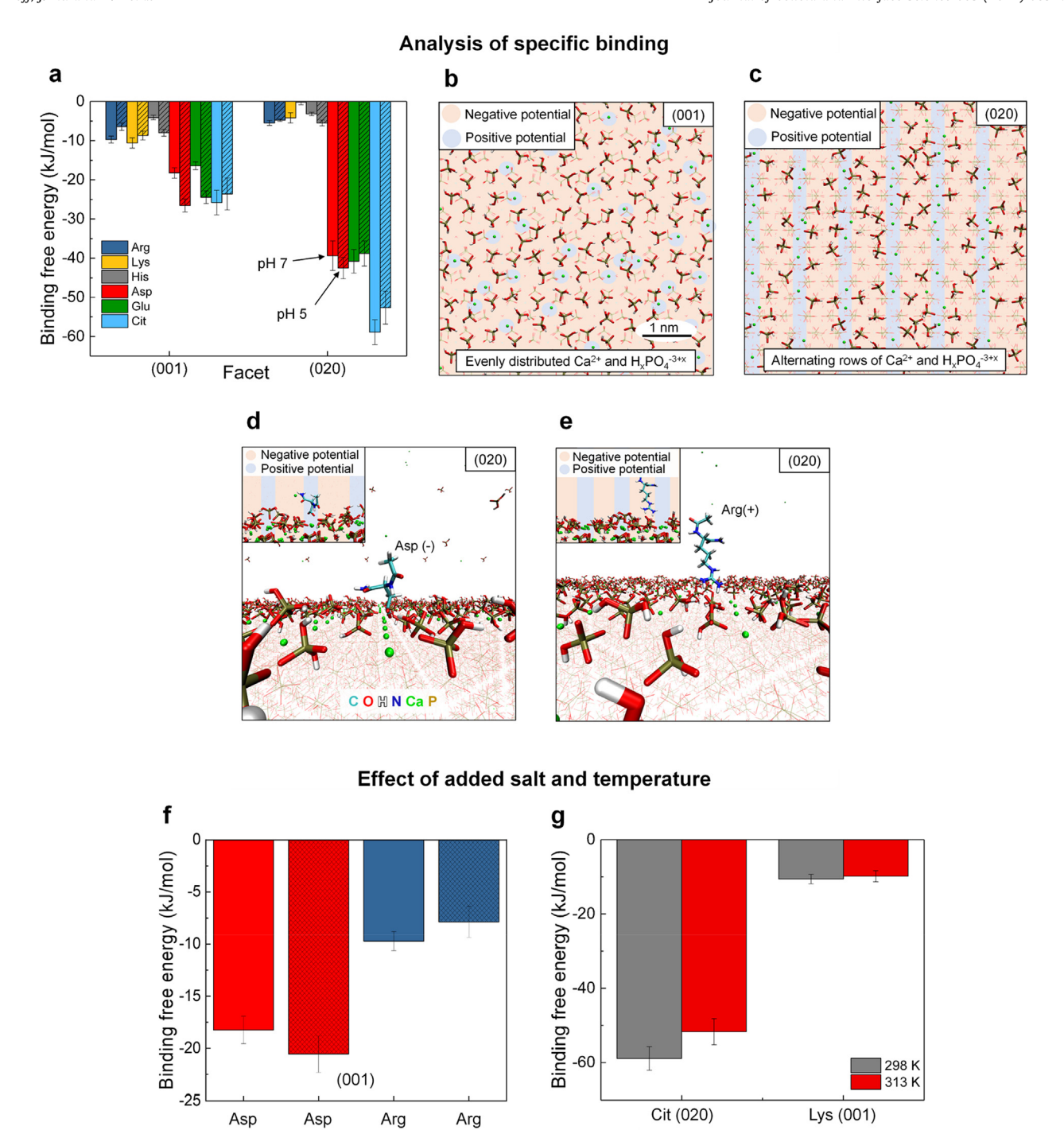


Fig. 6. Analysis of specific binding of charged amino acids and citrate to HAP (001) and (020) surfaces as a function of pH and the role of subsurface structure. Effects of added salt and temperature changes on the binding free energy are also shown. (a) Free energy of binding of charged amino acids and citrate at 298 K. Large differences are seen between (001) and (020) facets, as well as between positively and negatively charged amino acids. Error bars were determined using the bootstrap method. (b) Top view of the (001) HAP surface at pH 7. Areas of high phosphate density carry a negative charge and are shown with an orange background. Areas with high calcium density are shown with a blue background. A random distribution of calcium and protonated phosphate ions is seen, and an overall lower density of calcium ions than on the (020) surface results in more negative surface charge. (c) Top view of the (020) HAP surfaces at pH 7. The (020) surface exhibits rows of positive and negative potential. (d) A perspective view of aspartic acid D(-) binding to a calcium row in between phosphate rows on the (020) surface at pH 7. The inset shows how the binding position maximizes interactions of aspartic acid with areas of positive charge and reduces interactions with negative charge. (e) A perspective view of arginine R(+) on the (020) surface and interactions with phosphate species at pH 7. The inset shows R interactions with the negative potential area and some destabilization by nearby positive potential. (f) Free energies of binding of D and R on the (001) surface at pH 7 in water and in a 154 mM NaCl solution. The presence of salt has only minor effects on binding as the free energy of binding remains the same within the uncertainty (±3 kJ/mol). (g) Binding free energies of citrate and lysine on the (020) and (001) surfaces of HAP at pH 7 at 298 K and 313 K. The influence of temperature changes is within the uncertainty, potentially indicating a minor increase towards zero upon heating.

Amino acid and HAP facet

in water

in NaCl

in water

in NaCl

hydrogen bonds are formed between the nitrogen-bound hydrogen atoms and oxygen atoms in phosphate species on the surface. Their contribution to the binding free energy, however, is small as such H bonds form in exchange for pre-existing hydrogen bonds in solution before adsorption (Figure S5 in the Supplementary Material).

Negatively charged amino acids and citrate bind via carboxylate groups to exposed calcium ions on the HAP surface (Fig. 5d-f, j-l, Movie S2 in the Supplementary Material). This form of ion pairing involves strong, targeted ion pairs between –COO- groups and Ca²⁺ ions on the HAP surface. The ion pairs involve localization of the negative charge on 2 oxygen atoms and of the positive charge on single, divalent calcium ions, which leads to enhanced binding of negatively charged amino acids and citrate in comparison to the scenario of binding of positively charged amino acids to phosphate species with more distributed charge density. This difference amounts to between –7 and –33 kJ/mol on the (001) and (020) surfaces, respectively (Fig. 6a). Binding configurations of negatively charged amino acids also include hydrogen bonding to protonated phosphates, however, without a significant net contribution to binding free energies.

A distinctive pattern of binding strength is also seen for the (001) and (020) surfaces (Fig. 6a-e). The charge on the (001) surface is more negative compared to the (020) surface and more randomly distributed (Fig. 6b and Fig. 3c, e). The abundance of negatively charged phosphate species and less calcium ions on the (001) surface allows notable adsorption of positively charged amino acids R, K, and H(+) (Fig. 6a). The adsorption of negatively charged amino acids remains more favorable overall due to stronger ion pairs, even though less sites are available, and the attraction is clearly less than on the (020) surface (see also Fig. 2e, f, Fig. 5a-f). On the (020) surface, an alternating distribution of calcium ions and protonated phosphate ions creates rows of positive charge and negative charge (Fig. 6c and Fig. 3d, f). The presence of positive surface charge every 3 rows results in favorable binding conditions for negatively charged amino acids and citrate (see also Fig. 2g, h). The anionic molecules prefer binding to the rows of calcium ions in between rows of phosphate ions, which optimizes interactions with calcium ions and minimizes interactions with negatively charged $H_nPO_4^{-3+n}$ groups (Fig. 6d, Fig. 5j-1). In contrast, positively charged amino acids bind weakly to the rows with phosphate species (Fig. 6e, Fig. 5g-i). The higher fraction of area with positive charge on the (020) surface and decreased density of phosphate species of $\sim 75\%$ compared to the (001) surface (Fig. 6c-e) explain a \sim 60% decrease in binding free energy of K(+) and a $\sim 40\%$ decrease for R(+) relative to the (001) surface (Fig. 6a). The (020) surface thus has a relatively higher capacity for binding negatively charged amino acids and the (001) surface is more likely to facilitate a combined association with positively charged and negatively charged amino acids.

The free energy of binding ΔG is expected to be close to the enthalpy of binding ΔH due to moderate, or small entropy contributions $-T\Delta S$ ($\Delta G = \Delta H - T\Delta S$). A quantitative analysis is challenging since the dynamic surface structure of HAP complicates precise computations of binding enthalpies. We know, however, from closely related studies of peptide binding to static, chemically similar silica and calcium silicate surfaces (Si is the next neighbor of P in the periodic table) that it is common to observe 80% to 100% similarity of binding free energies and binding enthalpies [57,58,69]. The entropy contribution involves an entropy loss of the molecule upon surface binding and an entropy gain of displaced surfacebound water, which on balance is often close to zero or involves a small net entropy gain from release of water [70,71]. A typical scenario is therefore a slightly larger negative free energy of binding in comparison to the negative energy of binding (=enthalpy of binding in the absence of significant volume change).

2.6. Influence of pH Value, Salinity, and temperature

The influence of pH value in solution on the binding affinity is less significant than the influence of specific (hkl) facets. Nevertheless, a change in pH value from 7 to 5 modifies the surface chemistry, lowers the area density of calcium ions, and removes potential binding sites in a notable way (Fig. 1c, d). Dissolution and precipitation equilibria of phosphate species on the surface are accelerated towards pH 5. Positively charged amino acids R and K had a lower affinity to both (001) and (020) HAP surfaces at pH = 5 relative to pH = 7 as the phosphate species are then more extensively protonated and the negative surface charge is reduced (Fig. 6a). In contrast, the binding affinity of histidine increased on (001) and (020) surfaces as the pH value decreased from 7 to 5, nearly doubling on the (001) surface (Fig. 6a). The imidazolium side group then transitions from neutral to a positive charge (pK_a - \sim 6), and pH changes from 7 to 5 could be used as a reversible switch to tune the binding affinity of His and His-containing proteins.

Negatively charged amino acids are relatively inert with respect to the phosphate-rich (001) surface at medium distances at both pH values (Fig. 3a, c), or slightly repelled, and experience stronger binding as the pH value decreases from 7 to 5 (Fig. 6a). The shift towards stronger binding to the (001) surface at pH 5 is a result of the lower negative surface charge upon conversion of HPO $_4^2$ - ions into H₂PO $_4$ ions (Fig. 2e). The absolute binding affinity of citric acid remains about the same at pH 7 and pH 5, and herewith shifts from stronger than the negatively charged amino acids at pH = 7 to about equal affinity at pH = 5 (Fig. 6a). Accordingly, competition of the amino acids D and E with citric acid increases in low pH environments on the (001) surface.

The attraction of negatively charged amino acids to the Ca-rich (020) HAP surface remains about the same at pH 7 and 5 (Fig. 6a). The decrease in area density of superficial calcium ions upon transition from pH 7 to pH 5 is accompanied by a stoichiometric loss in superficial phosphate charge (Fig. 3a, d and Fig. 2g). Citrate clearly adsorbs stronger than the amino acids D and E on the (020) surface at pH 7 and at pH 5 (Fig. 6a).

Our analysis this far assumes adsorption in aqueous solution without significant electrolytes. Cations or anions were added only as needed to maintain overall charge neutrality. Therefore, we tested the effect of sodium chloride solutions at a nearphysiological concentration of 154 mM on the adsorption of D and R on the HAP (001) surface at pH 7 as examples (7Cl⁻ and 7Na⁺ ions added to \sim 2600 TIP3P water molecules) (Fig. 6f). The saline solution had a minor influence on the binding free energies. The phosphate-rich (001) HAP surface showed some binding of sodium ions, which can slightly increase the attraction of D(-) and reduce the attraction of R(+). The more charge-balanced Carich (020) surface did not attract Na⁺ ions nor Cl⁻ ions, suggesting no effects of sodium chloride addition on binding (see details in Section S2 in the Supplementary Material).

To examine the effect of temperature upon binding affinity, we computed the free energies of binding again at 313 K using citrate on (020) HAP surfaces and lysine on (001) HAP surfaces at pH 7 as examples (Fig. 6g). Cit and R represent the strongest negatively charged and positively charged binding species, respectively (Fig. 6a). The results indicate no major changes within the uncertainty (Fig. 6g) and similar trends are expected for other temperatures near physiological conditions.

2.7. Discussion of experimental data

Previous experimental data on amino acid and citrate affinity to HAP agree with the mechanisms identified by simulations, even though available at a rather simplistic level (rarely better than 1 nm resolution). The overall charge of a molecule was suggested as a principal factor in the strength of HAP surface interactions [72]. In experiment, a reduction in binding to HAP was observed when negatively charged poly-glutamic acid peptides were modified by changing Glu residues to non-charged Leu residues [8]. According to the simulation, a lower number of charged groups decreases the binding affinity to the surface (Fig. 2). Overall, there is consensus that negatively charged amino acids are the strongest binders to HAP, followed by either positively charged or polar amino acids [25-27,73]. Some studies, alternatively, mention that positively charged amino acids have higher affinity than negatively charged amino acids, since the latter experience repulsion from negatively charged HAP surfaces [21]. For example, lysine(+) bound stronger to carbonate-containing hydroxyapatite, which was attributed to a higher negative charge of the hydroxyapatite surface [21]. Both observations can be supported by our results (Figs. 2, 5, 6) since quantitative data, (hkl) specificity, and the influence of pH are not known in these experiments and leave uncertainty. According to the simulation, negatively charged amino acids are the strongest binders, followed by positively charged amino acids, and uncharged amino acids have little affinity. At the same time, positively charged amino acids can make significant binding contributions on (001) surfaces (Fig. 2), including differences as a function of distance from the surface (Fig. 3). Charge is the key factor to regulate binding of amino acids, combined with the structure and distribution of ions on the HAP surface.

The strong binding affinity of aspartic and glutamic acid in the simulation agrees with the known efficiency of acidic oligopeptides as bone binding sequences (Fig. 2) [74,75]. The formation of extended rod-like HAP crystals, reported experimentally in the presence of Asp [27], can be explained. Hereby, strong binding to the prismatic (020) facets inhibits growth along the a and b axes of hydroxyapatite, enabling faster growth along the c axis supporting the formation of rod-like crystals. Calcium ions must be accessible on the surface to enable strong binding of negatively charged ligands, and specific patterns of calcium ions on distinct (hkl) facets of HAP can be exploited to direct synthesis and assembly (Fig. 6). Peptides and synthetic ligands could be designed for high binding affinity by matching the average distance between calcium ions in near-linear patterns on the (020) surface at pH 7 (Fig. 6b, c). Vice versa, low area density and less regular spacing of calcium ions on the (001) surface can limit the amount of bound acidic (negatively charged) residues and favor positively charged residues (Fig. 6a).

The competition of acidic amino acids with citric acid for binding to HAP *in vivo* is also well known [76]. Citrate is abundantly found on apatite surfaces at concentrations of about 1 molecule per 2 nm². According to the simulation, citrate has the highest attraction to HAP among all tested species, -7 kJ/mol and -17 kJ/mol more favorable than D and E on the (001) and (020) surfaces at pH 7, respectively (Fig. 6a). The high affinity originates from the interaction with single or multiple calcium ions on the surface through multiple carboxylate groups and folding in between multiple protonated phosphate groups (Fig. 5f, I and Figure S1a, b in the Supplementary Material). More favorable binding to HAP surfaces than individual citrate molecules can be achieved through synergistic effects of several acidic ionic amino acids linked together in peptides and proteins.

Peptides derived from known HAP-binding proteins such as statherin and bone sialoprotein are known to control HAP growth [10]. The peptide sequences largely consist of acidic amino acid residues [11,77], and previous experiments have shown that Glu_6 peptides bind strongly to HAP while Glu_5 Leu and Glu_4 Leu $_2$ have increasingly weaker binding affinity [8,78]. These findings add evidence for the importance of acidic amino acids in HAP binding peptides. Stronger binding of more acidic amino acid sequences to HAP

concurs with the simulation results, especially to the abundant prismatic (010)/(020) facets with a higher positive surface charge than (001) facets (Fig. 2g, 3d, 6c).

Yet it is too simplistic to assume that negative residues alone are the key to HAP peptide binding as many unique HAP binding peptides sequences identified by phage display do not carry a large negative charge [2,14]. Recent studies discovered HAP binding peptides specific for (001) facets, including a strong binder (NNHYLPR), a medium(weak) binder (GQAGERK), and a weakest (WGNYAYK) binder. The peptides contain positively charged amino acids (R, K, H), and only the medium binder contains an additional negatively charged amino acid (E) [15]. The higher affinity of sequences containing positive charges to (001) surfaces is consistent with the specific charge profile at medium range and the reduced amount of Ca⁺ ions on the (001) surface (Fig. 2e, f, Fig. 3a. c. e. Fig. 6b). The lack of significantly acidic peptides from several phage display studies also demonstrates that peptide binding to HAP, or HAP nucleation from precursors, might not require the highest binding strength. Instead, mineralization processes may benefit from reversibility and are more complex than binding of individual amino acids.

2.8. Future opportunities

Amino acid binding is a fundamental molecular descriptor for rational design of peptides and proteins as part of more complex biomineral assembly processes. We revealed the role of the dynamic organization of phosphate species and Ca²⁺ ions on the HAP surface during dissolution-precipitation equilibria, leading to specific binding of amino acids as a function of (*hkl*) facet and pH value. The phosphate-based surfaces display much richer dynamics than silicates, clay, or titania, which is essential for the creation and dissolution of hierarchical skeletal structures.

An important factor are the chemical changes on the surface of hydroxyapatite. In this work, we considered acid-base reactions in the top molecular layer of hydroxyapatite. Further details of the interfacial structure will be worth exploring, for example, the influence of hydration and protonation of multiple molecular layers beneath the HAP surface. Layer-by-layer dissolution and precipitation may convert hydrated (001)/(002) surfaces into hydrated (004) surfaces, and hydrated (010)/(020) surfaces into hydrated (040) surfaces. At the same time, differences in directional patterns between (00n) and (0m0) surfaces, binding mechanisms, and trends in binding free energies would stay the same (Fig. 6).

Apatite models can be further extended to fluorapatite, chlorapatite, carbonate-containing HAP, and cation substitution commonly found in bone and teeth (e.g. Mg²+, Zn²+, Sr²+) [79]. In addition, the role of defects, step edges, and amorphous layers of calcium phosphate at mineral-solution interfaces would be interesting to explore in follow-on work, along with a broader range of concentration of amino acids and proteins (here we consider low concentrations of amino acids as a first step). Binding of bone-forming proteins such as osteocalcin, bone sialoprotein, collagen, and statherin could be accurately explored to combat bone-related disorders and diseases.

In such efforts, the MD methods using IFF have only a nominal computational cost, about ten million times lower than ab-initio methods. They can be applied for realistic computational and machine-learned design of biomolecules and phosphate surfaces for specific binding and assembly outcomes. The accuracy is several times higher than feasible before with prior models, and even large nanostructures of ~ 100 nm and time scales up to microseconds can be explored. Precise knowledge of the binding of building blocks such as amino acids is necessary towards rational understanding of observed binding patterns of peptides and proteins, to predict the effect of mutations for facet-specific binding and inform the syn-

thesis of new functional molecules. Applications may include targeting specific HAP crystal facets to inhibit or promote growth, deliver drugs to specific sites in bone and dentin, and utilize the dependence on pH value to target infectious mineral sites.

3. Conclusion

We examined the binding mechanism and adsorption free energies of all 20 natural, end-capped amino acids and citric acid on common hydroxyapatite surfaces as a function of pH value. We utilized an extensive series of over 1500 unrestrained and steered molecular dynamics simulations for pH-resolved surface models and diverse molecular start conformations with thoroughly validated force fields (IFF-CHARMM36). The simulation-based methods reveal quantitative details in all-atom, dynamic resolution which have remained elusive for decades, uncovering the design rules for specific recognition and new perspectives for the assembly of skeletal structures from the molecular scale.

Citrate ions, negatively charged amino acids (D, E), and positively charged amino acids (K, R, as well as H at pH 5) are the most significant binders to hydroxyapatite surfaces, up to -60 kJ/mol, while non-charged amino acids display marginal binding free energies around -2.5 kJ/mol. Thereby, the specific sequence of layers of ions and associated charge profiles for each (hkl) hydroxyapatite surface has a significant effect on the interaction with ionic amino acids at distances<1.2 nm. The affinity of the molecules to the HAP surface is determined by the ability to replace surface-bound water and to form ion pairs with calcium ions or protonated phosphate ions at close distances of < 0.3 nm from the top atomic layer. On the (010) and (020) surfaces, which constitute the prismatic plane of HAP crystals, citric acid binds significantly stronger than all amino acids, followed by the negatively charged amino acids, and positively charged amino acids exhibit less significant binding. A specific row-like pattern of phosphate species and calcium ions on the (010)/(020) surface can direct the assembly of adsorbed negatively charged molecules. The (001) surface, which constitutes the basal plane of HAP crystals, is less attractive to citrate ions and negatively charged amino acids related to a higher concentration of negative charge in the top atomic layer compared to the (010)/(020) surface. Positively charged amino acids thus exhibit increased binding to the (001) surface while binding by negatively charged amino acids and citrate ions still remains stronger.

The arrangement of calcium ions and protonated phosphate species at and below the (hkl) surface of hydroxyapatite affects the relative orientation and attraction of charged species. Small energy barriers between bound states and conformation in solution at distances < 1.2 nm were observed. Negatively charged molecules form stronger, more localized ion pairs with the HAP surface than positively charged amino acids, and effective binding is limited by the availability of calcium ions. Peptides with a mixture of positive and negative residues with an overall positive or zero charge may be more likely to target (001) surfaces due to a synergistic effect between the amino acids of various charge in comparison to highly anionic peptides, which would target (010)/(020) surfaces. A decrease in pH values from 7 to 5 augments binding of negatively charged amino acids and histidine on (001) surfaces and decreases the binding of other positively charged amino acids. Differences in binding free energies as a function of pH value are smaller on (020) surfaces due to a more balanced distribution of positive and negative charges, however, changes in the surface chemistry remain significant and reduce the overall availability of calcium ions from pH 7 to pH 5.

The results provide first quantitative guidance for sequence design, HAP shape control, and explain prior experimental findings on amino acid and peptide binding to HAP in a new light and in an unprecedented level of detail. Most notably, the resolution in the

simulation (1–5 pm) is about 100 times higher than that of current imaging techniques (0.1–2 nm), which typically cannot provide specific binding information, facet-specific and pH-specific detail. Therefore, the IFF-MD based methods fill a major gap in current instrumentation by capturing critical recognition mechanisms and interfacial dynamics, consistent with available data from spectroscopy, acid-base chemistry, hydration measurements, and biomolecular interactions [36]. Beyond the specific results for amino acids and citrate ions, the models and simulation methods facilitate the examination of specific binding of other molecules and mineralization of phosphate minerals, of the role of proteins, electrolyte composition, and assembly mechanisms in combination with laboratory studies.

4. Computational methods

4.1. Simulation setup

Models for hydroxyapatite (001) and (020) surfaces were constructed using X-ray data and surface chemistry according to the pH values as described in the IFF surface model database (Fig. 1b-d) [36,37]. We employed the Graphical User Interface of the Materials Studio program [80]. As the pH value decreases, hydroxvapatite surfaces undergo a series of chemical reactions, which change the area density and protonation state of the charged species in the first molecular layers of the surface. These reactions include hydroxide neutralization at pH < 15, successive protonation of phosphate ions, and dissolution of calcium ions for pH values from 13 to 1 according to known pK values. The area density of calcium ions and negative surface charge change drastically as a function of the chosen conditions (Fig. 1b-d). The hydroxyapatite dimensions of roughly 37.66×8 (001) surfaces had $32.621 \times 28 \text{ Å}^3$ and the (020) surfaces dimensions of roughly $37.668 \times 34.375 \times 34 \, \text{Å}^3$. A slab of $\sim 2600 \, \text{TIP3P}$ water molecules of approximately 60 Å height was added above the HAP surface. These dimensions ensure the absence of interactions between amino acids in periodic neighbor cells, corresponding to dilute concentration. The protonation state of the HAP surface at pH 7 was represented by a mixture of 70% H₂PO₄ ions and 30% HPO₄²⁻ ions in the top molecular layer, and at pH 5 by 100% H₂PO₄ ions in the top molecular layer [36,37]. Accordingly, the first molecular layer of phosphate species on every surface was protonated in the correct stoichiometric ratio of $H_2PO_4^-$ ions and HPO_4^{2-} ions according to pH value (no PO₄³ ions and no H₃PO₄ molecules

Models of amino acids and citrate ions were also prepared using the Materials Studio Visualizer [80]. Amino acids were end-capped with an acylated N-terminal and an amidated C-terminal to represent amino acid chemistry within a peptide or protein. The inclusion of approximately 2600 water molecules using the TIP3P water model leads to a nominal concentration of ~ 20 mM. The effective concentration can be considered many times lower as the 3D periodic simulation box allows no aggregation.

The different HAP surfaces were solvated in TIP3P water at 298.15 K and at 1 atm and initially simulated for at least 30 ns in the NPT ensemble to ensure thorough equilibration including the water slab of ~ 60 Å thickness in contact with the mineral surface. Then, the HAP surfaces were combined with the capped amino acids and counter ions, including chloride and sodium, as necessary to maintain charge neutrality (1Cl $^-$ ion for K (+), R(+), H(+), 1Na $^+$ ion for D(-), E(-), and 2 or 3Na $^+$ ions for Cit (-2, -3)). The protonation states of citrate and histidine were adjusted according to the pH value, including Cit(-3) and His(0) at pH = 7, and Cit(-2) and His(+) at pH = 5. In the combined systems of hydroxyapatite, water, and organic molecules, two phosphate atoms in the middle of the

HAP slab were restrained during all steered molecular dynamics simulations.

We utilized the IFF-CHARMM36 force field for hydroxyapatite, the amino acids, citrate, and water. The energy expression utilizes bonded terms, atomic charges, and a 12–6 Lennard-Jones potential for nonbonded interactions [37,69]. Molecular dynamics simulations were carried out using the NAMD program[81] in the NPT ensemble at 298.15 K with the Langevin thermostat and piston to maintain a constant pressure at 1 atm. The time step was 1 fs in all simulations. A 12 Å cutoff was applied to nonbonded interactions including a force switching function at 10 Å. (The results are equal to using a straight 12 Å cutoff for LJ interactions with<1% difference in computed energies). Electrostatic interactions beyond 12 Å distance were calculated using the particle-mesh Ewald method in high accuracy using a tolerance of 10^{-6} .

4.2. Steered molecular dynamics simulation

Steered molecular dynamics (SMD) simulations from bulk solution to the surface were conducted for all 20 amino acids and citrate ions on the (001) and (020) surfaces at pH values and 5 and 7 (Fig. 1a). Each run began with the amino acid's center of mass (COM) at least 15 Å away from the average protonated phosphate position on the top layer of the respective equilibrated hydroxyapatite surface. The capped amino acids were constrained at their respective COM position in the z direction to a harmonic spring with a spring constant of 60 kcal/(mol·Å²) to ensure that a stiff spring approximation could be applied (Figure S6 in the Supplementary Material) [82]. The COM was pulled using a constant velocity of 1 Å/ns towards the surface in the z direction in the NPT ensemble. SMD simulations were repeated a minimum of four times for each amino acid. The force required to restrain the amino acid at a given time step was recorded and the resulting change in work from state 3 in solution to state 1 on the HAP surface (Fig. 1a) was used to determine the relative order of affinity towards the surfaces and stable conformations on the HAP surfaces.

4.3. Unrestrained molecular dynamics

Unrestrained MD simulations were used to increase the sampling of conformations of the amino acids on the surface and allow them to settle into favorable conformations. In particular, charged, capped amino acids were studied in unrestrained molecular dynamics simulations in the NPT ensemble with a duration of $\gg 6$ ns at 298.15 K and 1 atm pressure. A minimum of four configurations of Asp, Glu, Arg, and Lys were subjected to unrestrained MD simulations starting from the most favorable minimum free energy configurations taken from the previous SMD simulations. Additional simulations with individual Asp, Glu, Arg, Lys, His, and citrate molecules placed in solution and near the surface were performed to allow the molecules to find stable conformations on the surface separate from the previous SMD runs.

4.4. Free energy calculations

Stable binding conformations from unrestrained MD simulations as well as solution-to-surface SMD simulations were selected as starting configurations for surface-to-solution SMD simulations. These SMD simulations in the reverse direction were carried out with the same specifications as the previous SMD simulations. A minimum of 4 different start structures were selected, and the free energy of binding for each of the 20 amino acids was calculated using the Jarzynski Equality exponential method (Equation (1)) over a series of 12 to 28 runs, with three runs per start structure: [83,84]

$$\langle e^{-\beta W_{AB}} \rangle = e^{-\beta \Delta G_{AB}}$$
 (1)

Hereby, W_{AB} is the total work of desorption (or adsorption), from minimum to steady values at large distance, β is equal to 1/RT, and ΔG is the free energy resulting as a thermodynamic statistical average. The set of work profiles for arginine on the (001) surface at pH 7, and isoleucine on the (020) surface at pH 7 are shown as examples (Figures S7 and S8 in the Supplementary Material). The purpose of carrying out at least three simulations per conformation was to determine whether the initial starting conformation for the SMD runs was in equilibrium or a higher energy minimum. Over a single SMD run it would not be possible to determine whether the starting conformation was in equilibrium, out of equilibrium (not the most favorable conformation), or if the amino acid has an inherently low binding affinity towards the HAP surface.

To further validate the precision of the free energy calculations, the Forward/Reverse method [85] was used to calculate the free energy for Arg, and Lys at the (001) and (020) surfaces at both pH 5 and 7, as well as for Asp on the (001) surface at pH 7. We combined the previous solution-to-surface SMD simulations with the surface-to-solution SMD simulations when the amino acid had the same binding conformations. The results led to the same qualitative trends in amino acid binding affinity and values within error to those reported from the exponential method. An exception was Arg on the (001) surface at pH = 7, which had a slightly larger deviation, yet still <±3 kJ/mol (Figure S9 in the Supplementary Material). Specific care was taken to ensure that, for trajectories used in the analysis, structures were at equilibrium on the HAP surfaces at the beginning of SMD simulations, similar binding conformations and pathways were used, and sufficient sampling was allowed. Prior to surface-to-solution SMD runs, the sampling of representative, low-energy conformations of amino acids was critical to obtain low errors using a limited number of simulations (12 to 28). In total, >1500 SMD simulations were carried out for all systems. These include combinations of 4 types of surfaces, 20 amino acids, citrate, added NaCl electrolyte and different temperatures, forward and reverse simulations, and 12 to 28 repeats for each system to compute accurate free energies of binding.

4.5. Uncertainties

The error bars of computed free energies were obtained using bootstrap sampling on the SMD work profiles in the Jarzynski and Forward/Reverse methods (see Section S1.3 in the Supplementary Material), which is similar in reliability to comparing differences in block averages [70,71]. The uncertainties are generally on the order of kT, or in the low percent range. Further indicators are the fluctuations in binding free energies for neutral (non-binding) amino acids (Fig. 2a-d), as well as the sensitivity to changes in salinity and temperature (Fig. 6f, g).

The reliability of SMD for calculating interfacial energies was recently compared to umbrella sampling and well-tempered metadynamics [86]. Hereby, it was shown that SMD can overestimate the negative binding free energy of molecules (e.g. water) on highly ionic surfaces when typical pulling velocities (1 Å/ns) are applied. Uncertainties with SMD can be lowered by decreasing SMD pulling velocities until free energies become independent of the pulling velocity (e.g. 0.1 Å/ns or 0.01 Å/ns) [87], and if not possible, by switching to umbrella sampling or well-tempered metadynamics. Specifically, Wei et al. [86] employed SMD to study water adsorption on a "hypothetical" hydroxyapatite surface with overestimated atomic charges q of Ca of + 2.0e (recommended value: $\pm 1.5 \pm 0.1e$), P of $\pm 2.6e$ (recommended value: $\pm 0.8e$ to + 1.0e), O, and a high area density of ions at pH > 14 (typical values: 3 to 10) [36,52]. Free energies of binding from SMD were then too large relative to more accurate values by umbrella sampling and well-tempered metadynamics [86]. In this scenario, the high atomic charges cause excessive attraction of water to superficial

calcium and phosphate ions (which scales with q^2), magnify energy barriers, and make sampling by SMD very challenging. These situations do not apply in the present work, which involved shallower energy barriers for adsorption on the HAP surfaces due to realistic atomic charges and lower ion densities at pH 7 and 5.

Declaration of Competing Interest

The authors declare that they have no known competing financial interests or personal relationships that could have appeared to influence the work reported in this paper.

Acknowledgement

This work was supported by the National Science Foundation (DMREF-1623947, CBET-1530790, OAC 1931587), and the University of Colorado-Boulder. We acknowledge computing resources at the Summit Supercomputer, a joint effort of the University of Colorado Boulder and Colorado State University, which is supported by the National Science Foundation (ACI-1532235 and ACI-1532236), as well as resources at the Argonne Leadership Computing Facility, which is a DoE Office of Science User Facility supported under Contract DE-AC02-06CH11357.

Author contributions

HH conceived the study. SH and JL carried out simulations. SH, JL, and HH wrote the paper.

Appendix A. Supplementary data

Supplementary data to this article can be found online at https://doi.org/10.1016/j.jcis.2021.07.109.

References

- [1] B. Clarke, Normal Bone Anatomy and Physiology, Clin. J. Am. Soc. Nephrol. 3 Supplement 3) (2008) S131-S139.
- [2] M.D. Roy, S.K. Stanley, E.J. Amis, M.L. Becker, Identification of a Highly Specific Hydroxyapatite-Binding Peptide Using Phage Display, Adv. Mater. 20 (2008) 1830-1836.
- S. Koutsopoulos, E. Dalas, Hydroxyapatite Crystallization in the presence of Serine, Tyrosine and Hydroxyproline Amino Acids with Polar Side Groups, J. Cryst. Growth 216 (2000) 443-449.
- M.C. Weiger, J.J. Park, M.D. Roy, C.M. Stafford, A. Karim, M.L. Becker, Quantification of the Binding Affinity of a Specific Hydroxyapatite Binding Peptide, Biomaterials 31 (2010) 2955-2963.
- [5] W.J. Chung, K.Y. Kwon, J. Song, S.W. Lee, Evolutionary Screening of Collagenlike Peptides That Nucleate Hydroxyapatite Crystals, Langmuir 27 (2011) 7620-7628.
- [6] V.K. Sharma, M. Johnsson, J.D. Sallis, G.H. Nancollas, Influence of Citrate and Phosphocitrate on the Crystallization of Octacalcium Phosphate, Langmuir 8 2) (1992) 676–679.
- Y.-Y. Hu, X.P. Liu, X. Ma, A. Rawal, T. Prozorov, M. Akinc, S.K. Mallapragada, K. Schmidt-Rohr, Biomimetic Self-Assembling Copolymer-Hydroxyapatite Nanocomposites with the Nanocrystal Size Controlled by Citrate, Chem. Mater. 23 (9) (2011) 2481–2490.
- [8] R. Fujisawa, Y. Wada, Y. Nodasaka, Y. Kuboki, Acidic Amino Acid-Rich Sequences as Binding Sites of Osteonectin to Hydroxyapatite Crystals, Biochim. Biophys. Acta, Protein Struct. Mol. Enzymol. 1292 (1) (1996) 53-60.
- G. He, T. Dahl, A. Veis, A. George, Nucleation of Apatite Crystals in vitro by Self-Assembled Dentin Matrix Protein 1, Nat. Mater. 2 (8) (2003) 552–558.
- [10] J.R. Long, J.L. Dindot, H. Zebroski, S. Kiihne, R.H. Clark, A.A. Campbell, P.S. Stayton, G.P. Drobny, A Peptide that Inhibits Hydroxyapatite Growth is in an Extended Conformation on the Crystal Surface, Proc. Natl. Acad. Sci. U. S. A. 95 21) (1998) 12083-12087.
- [11] R. Fujisawa, M. Mizuno, Y. Nodasaka, K. Yoshinori, Attachment of Osteoblastic Cells to Hydroxyapatite Crystals by a Synthetic Peptide (Glu(7)-Pro-Arg-Gly-Asp-Thr) Containing Two Functional Sequences of Bone Sialoprotein, Matrix biology: journal of the International Society for Matrix Biology 16 (1) (1997)
- [12] D. Itoh, S. Yoneda, S. Kuroda, H. Kondo, A. Umezawa, K. Ohya, T. Ohyama, S. Kasugai, Enhancement of Osteogenesis on Hydroxyapatite Surface Coated with

- Synthetic Peptide (EEEEEEPRGDT) in vitro, J. Biomed. Mater. Res. 62 (2) (2002)292-298
- [13] W.J. Shaw, J.R. Long, J.L. Dindot, A.A. Campbell, P.S. Stayton, G.P. Drobny, Determination of Statherin N-Terminal Peptide Conformation Hydroxyapatite Crystals, J. Am. Chem. Soc. 122 (8) (2000) 1709-1716.
- [14] M. Gungormus, H. Fong, I.W. Kim, J.S. Evans, C. Tamerler, M. Sarikaya, Regulation of In Vitro Calcium Phosphate Mineralization by Combinatorially Selected Hydroxyapatite-Binding Peptides, Biomacromolecules 9 (3) (2008) 966-973
- [15] J. Mao, X. Shi, Y.-B. Wu, S.-Q. Gong, Identification of Specific Hydroxyapatite 001 Binding Heptapeptide by Phage Display and Its Nucleation Effect, Materials 9 (8) (2016) 700, https://doi.org/10.3390/ma9080700.
- [16] X. Chu, W. Jiang, Z. Zhang, Y. Yan, H. Pan, X. Xu, R. Tang, Unique Roles of Acidic Amino Acids in Phase Transformation of Calcium Phosphates, J. Phys. Chem. B 115 (5) (2011) 1151-1157.
- Y. Cai, R. Tang, Calcium Phosphate Nanoparticles in Biomineralization and Biomaterials, J. Mater. Chem. 18 (32) (2008) 3775, https://doi.org/10.1039/
- [18] T. Matsumoto, M. Okazaki, M. Inoue, Y. Hamada, M. Taira, J. Takahashi, Crystallinity and Solubility Characteristics of Hydroxyapatite Adsorbed Amino Acid, Biomaterials 23 (10) (2002) 2241–2247.
- [19] M.T. Jahromi, G. Yao, M. Cerruti, The Importance of Amino Acid Interactions in the Crystallization of Hydroxyapatite, J. R, Soc. Interface 10 (80) (2013) 20120906, https://doi.org/10.1098/rsif.2012.0906.
- [20] B. Palazzo, D. Walsh, M. Iafisco, E. Foresti, L. Bertinetti, G. Martra, C.L. Bianchi, G. Cappelletti, N. Roveri, Amino Acid Synergetic Effect on Structure, Morphology and Surface Properties of Biomimetic Apatite Nanocrystals, Acta Biomater. 5 (4) (2009) 1241–1252.
- [21] K.S. Jack, T.G. Vizcarra, M. Trau, Characterization and Surface Properties of Amino-Acid-Modified, Carbonate-Containing Hydroxyapatite Langmuir 23 (24) (2007) 12233–12242.
- [22] Z. Wang, Z. Xu, W. Zhao, N. Sahai, A Potential Mechanism for Amino Acid-Controlled Crystal Growth of Hydroxyapatite, J. Mater. Chem. B 3 (47) (2015)
- [23] R.W. Friddle, K. Battle, V. Trubetskoy, J. Tao, E.A. Salter, J. Moradian-Oldak, J.J. De Yoreo, A. Wierzbicki, Single-Molecule Determination of the Face-Specific Adsorption of Amelogenin's C-Terminus on Hydroxyapatite, Angew. Chem.-Int. Edit. 50 (33) (2011) 7541-7545.
- [24] H. Tanaka, M. Chikazawa, K. Kandori, T. Ishikawa, Influence of Thermal Treatment on the Structure of Calcium Hydroxyapatite, Phys. Chem. Chem. Phys. 2 (11) (2000) 2647-2650.
- [25] S. Koutsopoulos, E. Dalas, The Effect of Acidic Amino Acids on Hydroxyapatite Crystallization, J. Cryst. Growth 217 (4) (2000) 410-415.
- [26] S. Koutsopoulos, E. Dalas, Inhibition of Hydroxyapatite Formation in Aqueous Solutions by Amino Acids with Hydrophobic Side Groups, Langmuir 16 (2000) 6739-6744.
- [27] R. Gonzalez-McQuire, J.Y. Chane-Ching, E. Vignaud, A. Lebugle, S. Mann, Synthesis and Characterization of Amino Acid-Functionalized Hydroxyapatite Nanorods, J. Mater. Chem. 14 (2004) 2277–2281.
- [28] S.V. Patwardhan, F.S. Emami, R.J. Berry, S.E. Jones, R.R. Naik, O. Deschaume, H. Heinz, C.C. Perry, Chemistry of Aqueous Silica Nanoparticle Surfaces and the Mechanism of Selective Peptide Adsorption, J. Am. Chem. Soc. 134 (2012) 6244-6256.
- [29] H. Heinz, Clay Minerals for Nanocomposites and Biotechnology: Surface Modification, Dynamics and Responses to Stimuli, Clay Miner. 47 (2012) 205-230.
- [30] Z.C. Zhang, Q.G. Lai, Y.N. Li, C. Xu, X.P. Tang, J.B. Ci, S.L. Sun, B.B. Xu, Y. Li, Acidic pH Environment Induces Autophagy in Osteoblasts, Sci. Rep. 7 (2017) 46161.
- [31] N. Almora-Barrios, K.F. Austen, N.H. de Leeuw, Density Functional Theory Study of the Binding of Glycine, Proline, and Hydroxyproline to the Hydroxyapatite (0001) and (01–10) Surfaces, Langmuir 25 (2009) 5018–5025.
- [32] H.H. Pan, J.H. Tao, X.R. Xu, R.K. Tang, Adsorption Processes of Gly and Glu Amino Acids on Hydroxyapatite Surfaces at the Atomic Level, Langmuir 23 (2007) 8972-8981.
- [33] M. Corno, A. Rimola, V. Bolis, P. Ugliengo, Hydroxyapatite as a Key Biomaterial:
- Quantum-Mechanical Simulation of its Surfaces in Interaction with Biomolecules, Phys. Chem. Chem. Phys. 12 (2010) 6309–6329.

 [34] Z.Y. Lou, Q. Zeng, X. Chu, F. Yang, D.W. He, M.L. Yang, M.L. Xiang, X.D. Zhang, H. S. Fan, First-Principles Study of the Adsorption of Lysine on Hydroxyapatite (100) Surface, Appl. Surf. Sci. 258 (2012) 4911-4916.
- [35] Z. Xu, Y. Yang, Z. Wang, D. Mkhonto, C. Shang, Z.P. Liu, Q. Cui, N. Sahai, Small Molecule-Mediated Control of Hydroxyapatite Growth: Free Energy Calculations Benchmarked to Density Functional Theory, J. Comput. Chem. 35 (2014) 70-81.
- [36] T.-J. Lin, H. Heinz, Accurate Force Field Parameters and pH Resolved Surface Models for Hydroxyapatite to Understand Structure, Mechanics, Hydration, and Biological Interfaces, Journal of Physical Chemistry C 120(9)(2016) 4975–4992.
- [37] H. Heinz, T.-J. Lin, R. Kishore Mishra, F.S. Emami, Thermodynamically Consistent Force Fields for the Assembly of Inorganic, Organic, and Biological Nanostructures: The INTERFACE Force Field, Langmuir 29 (6) (2013) 1754-1765.
- [38] A. Garley, S.E. Hoff, N. Saikia, S. Jamadagni, A. Baig, H. Heinz, Adsorption and Substitution of Metal Ions on Hydroxyapatite as a Function of Crystal Facet and Electrolyte pH, J. Phys. Chem. C 123 (27) (2019) 16982-16993.
- W. Zhao, Z. Xu, Q. Cui, N. Sahai, Predicting the Structure-Activity Relationship of Hydroxyapatite-Binding Peptides by Enhanced-Sampling Molecular Simulation, Langmuir 32 (27) (2016) 7009-7022.

- [40] S. Hauptmann, H. Dufner, J. Brickmann, S.M. Kast, R.S. Berry, Potential Energy Function for Apatites, Phys. Chem. Chem. Phys. 5 (3) (2003) 635–639.
- [41] M. Aning, D.O. Welch, B.S.H. Royce, The Surface Energy of Fluorapatite, Phys. Lett. A 37 (1971) 253–254.
- [42] H.M. Rootare, R.G. Craig, Free Surface Energy Change for Water Adsorbed on Hydroxyapatite, J. Dental Res. 56 (1977) 744–747.
- [43] S.S. Barton, B.H. Harrison, Surface Properties of Hydroxyapatites. I. Enthalpy of Immersion, J. Colloid Interface Sci. 55 (1976) 409–414.
- [44] H.M. Rootare, R.G. Craig, Vapor Phase Adsorption of Water on Hydroxyapatite, J. Dental Res. 56 (1977) 1437–1448.
- [45] S. Brunauer, D.L. Kantro, C.H. Weise, The Surface Energies of Calcium Oxide and Calcium Hydroxide, Can. J. Chem. 34 (1956) 729–742.
- [46] S. Brunauer, D.L. Kantro, C.H. Weise, The Surface Energy of Tobermorite, Can. J. Chem. 37 (1959) 714–724.
- [47] M.L. Oglesby, P.L. Gutshall, J.M. Phillips, Cleavage Surface Energy of Selenite, Am. Mineral. 61 (1976) 295–298.
- [48] J.W. Shen, T. Wu, Q. Wang, H.H. Pan, Molecular Simulation of Protein Adsorption and Desorption on Hydroxyapatite Surfaces, Biomaterials 29 (2008) 513–532.
- [49] C. Tamerler, M. Sarikaya, Molecular Biomimetics: Nanotechnology and Bionanotechnology using Genetically Engineered Peptides, Philos. Trans. R. Soc., A, 367 (2009) 1705-1726.
- [50] V.G. Ruiz, W. Liu, A. Tkatchenko, Density-Functional Theory with Screened van der Waals Interactions Applied to Atomic and Molecular Adsorbates on Close-Packed and Non-Close-Packed Surfaces, Phys. Rev. B 93 (2016) 035118.
- [51] Y. Wang, P. Verma, X. Jin, D.G. Truhlar, X. He, Revised M06 Density Functional for Main-Group and Transition-Metal Chemistry, Proc. Natl. Acad. Sci. U. S. A. 115 (2018) 10257–10262.
- [52] H. Heinz, U.W. Suter, Atomic Charges for Classical Simulations of Polar Systems, J. Phys. Chem. B 108 (2004) 18341–18352.
- [53] Y.-X. Ma, S.E. Hoff, X.-Q. Huang, J. Liu, Q.-Q. Wan, Q. Song, J.-T. Gu, H. Heinz, F.R. Tay, L.-N. Niu, Involvement of Prenucleation Clusters in Calcium Phosphate Mineralization of Collagen, Acta Biomater. 120 (2020) 213–223.
- [54] F.S. Emami, V. Puddu, R.J. Berry, V. Varshney, S.V. Patwardhan, C.C. Perry, H. Heinz, Force Field and a Surface Model Database for Silica to Simulate Interfacial Properties in Atomic Resolution, Chem. Mater. 26 (2014) 2647– 2658
- [55] L.O. Mark, C. Zhu, J.W. Medlin, H. Heinz, Understanding the Surface Reactivity of Ligand-Protected Metal Nanoparticles for Biomass Upgrading, ACS Catal. 10 (2020) 5462–5474.
- [56] I.L. Geada, H. Ramezani-Dakhel, T. Jamil, M. Sulpizi, H. Heinz, Insight into Induced Charges at Metal Surfaces and Biointerfaces Using a Polarizable Lennard-Jones Potential, Nat. Comm. 9 (2018) 716.
- [57] F.S. Emami, V. Puddu, R.J. Berry, V. Varshney, S.V. Patwardhan, C.C. Perry, H. Heinz, Prediction of Specific Biomolecule Adsorption on Silica Surfaces as a Function of pH and Particle Size, Chem. Mater. 26 (2014) 5725–5734.
- [58] T. Jamil, A. Javadi, H. Heinz, Mechanism of Molecular Interaction of Acrylate-Polyethylene Glycol Acrylate Copolymers with Calcium Silicate Hydrate Surfaces, Green Chem. 22 (2020) 1577–1593.
- [59] J. Liu, J. Zeng, C. Zhu, J. Miao, Y. Huang, H. Heinz, Interpretable Molecular Models for Molybdenum Disulfide and Insight into Selective Peptide Recognition, Chem. Sci. 11 (2020) 8708–8722.
- [60] C. Pramanik, T. Jamil, J.R. Gissinger, D. Guittet, P.J. Arias-Monje, S. Kumar, H. Heinz, Polyacrylonitrile Interactions with Carbon Nanotubes in Solution: Conformations and Binding as a Function of Solvent, Temperature, and Concentration, Adv. Funct. Mater. 29 (2019) 1905247.
- [61] L. Ruan, H. Ramezani-Dakhel, C. Lee, Y. Li, X. Duan, H. Heinz, Y.u. Huang, A Rational Biomimetic Approach to Structure Defect Generation in Colloidal Nanocrystals, Acs Nano 8 (7) (2014) 6934–6944.
- [62] B.D. Briggs, N.M. Bedford, S. Seifert, H. Koerner, H. Ramezani-Dakhel, H. Heinz, R.R. Naik, A.I. Frenkel, M.R. Knecht, Atomic-Scale Identification of Pd Leaching in Nanoparticle Catalyzed CC Coupling: Effects of Particle Surface Disorder, Chem. Sci. 6 (11) (2015) 6413–6419.
- [63] Z. Xu, Q. Wei, W. Zhao, Q. Cui, N. Sahai, Essence of Small Molecule-Mediated Control of Hydroxyapatite Growth: Free Energy Calculations of Amino Acid Side Chain Analogues, J. Phys. Chem. C 122 (8) (2018) 4372–4380.
- [64] F. Dickens, The Citric Acid Content of Animal Tissues, with Reference to its Occurrence in Bone and Tumor, Biochem. J. 35 (1941) 1011–1023.
- [65] C.C. Dharmawardhana, K. Kanhaiya, T.-J. Lin, A. Garley, M.R. Knecht, J. Zhou, J. Miao, H. Heinz, Reliable Computational Design of Biological-Inorganic

- Materials to the Large Nanometer Scale Using Interface-FF, Mol. Sim. 43 (13-16) (2017) 1394–1405
- [66] H. Heinz, H. Koerner, K.L. Anderson, R.A. Vaia, B.L. Farmer, Force Field for Mica-Type Silicates and Dynamics of Octadecylammonium Chains Grafted to Montmorillonite, Chem. Mater. 17 (23) (2005) 5658–5669.
- [67] Y.-T. Fu, G.D. Zartman, M. Yoonessi, L.F. Drummy, H. Heinz, Bending of Layered Silicates on the Nanometer Scale: Mechanism, Stored Energy, and Curvature Limits, J. Phys. Chem. C 115 (45) (2011) 22292–22300.
- [68] CRC Handbook of Chemistry and Physics, 101st ed., CRC Press, Boca Raton, FL, 2020
- [69] H. Heinz, H. Ramezani-Dakhel, Simulations of Inorganic-Bioorganic Interfaces to Discover New Materials: Insights, Comparisons to Experiment, Challenges, and Opportunities, Chem. Soc. Rev. 45 (2) (2016) 412–448.
- [70] J. Feng, J.M. Slocik, M. Sarikaya, R.R. Naik, B.L. Farmer, H. Heinz, Influence of the Shape of Nanostructured Metal Surfaces on Adsorption of Single Peptide Molecules in Aqueous Solution, Small 8 (7) (2012) 1049–1059.
- [71] J. Feng, R.B. Pandey, R.J. Berry, B.L. Farmer, R.R. Naik, H. Heinz, Adsorption Mechanism of Single Amino Acid and Surfactant Molecules to Au 111 Surfaces in Aqueous Solution: Design Rules for Metal-Binding Molecules, Soft Matter 7 (2011) 2113–2120.
- [72] W.N. Addison, S.J. Miller, J. Ramaswamy, A. Mansouri, D.H. Kohn, M.D. Mckee, Phosphorylation-dependent Mineral Type Specificity for Apatite Binding Peptide Sequences, Biomaterials 31 (2010) 9422–9430.
- [73] E. Dalas, P. Malkaj, Z. Vasileiou, D.G. Kanellopoulou, The Effect of Leucine on the Crystal Growth of Calcium Phosphate, J. Mater Sci.-Mater. M. 19 (2008) 277–282.
- [74] T. Nishioka, S. Tomatsu, M.A. Gutierrez, K. Miyamoto, G.G. Trandafirescu, P.L.C. Lopez, J.H. Grubb, R. Kanai, H. Kobayashi, S. Yamaguchi, G.S. Gottesman, R. Cahill, A. Noguchi, W.S. Sly, Enhancement of Drug Delivery to Bone: Characterization of Human Tissue-Non Specific Alkaline Phosphatase Tagged with an Acidic Oligopeptide, Mol. Genet. Metab. 88 (2006) 244–255.
- [75] J.L. Millan, S. Narisawa, I. Lemire, T.P. Loisel, G. Boileau, P. Leonard, S. Gramatikova, R. Terkeltaub, N.P. Camacho, M.D. Mckee, P. Crine, M.P. Whyte, Enzyme Replacement Therapy for Murine Hypophosphatasia, J. Bone Miner. Res. 23 (2008) 777–787.
- [76] Y.-Y. Hu, A. Rawal, K. Schmidt-Rohr, Strongly Bound Citrate Stabilizes the Apatite Nanocrystals in Bone, Proc. Natl. Acad. Sci. U. S. A. 107 (52) (2010) 22425–22429.
- [77] K. Wikiel, E.M. Burke, J.W. Perich, E.C. Reynolds, G.H. Nancollas, Hydroxyapatite Mineralization and Demineralization in the Presence of Synthetic Phosphorylated Pentapeptides, Arch. Oral Biol. 39 (8) (1994) 715– 721.
- [78] J.S. Lee, X. Yu, A.J. Wagoner Johnson, W.L. Murphy, Mineral Binding Peptides with Enhanced Binding Stability in Serum, Biomater. Sci. 5 (4) (2017) 663–668.
- [79] K. Pajor, L. Pajchel, J. Kolmas, Hydroxyapatite and Fluorapatite in Conservative Dentistry and Oral Implantology-A Review, Materials 12 (17) (2019) 2683, https://doi.org/10.3390/ma12172683.
- [80] M. Studio, Program Suite and User Guide, Biovia/Dassault Systemes, Cambridge, UK, 2019, p. 2019.
- [81] J.C. Phillips, R. Braun, W. Wang, J. Gumbart, E. Tajkhorshid, E. Villa, C. Chipot, R. D. Skeel, L. Kale, K. Schulten, Scalable Molecular Dynamics with NAMD, J. Comput. Chem. 26 (2005) 1781–1802.
- [82] S. Park, F. Khalili-Araghi, E. Tajkhorshid, K. Schulten, Free Energy Calculation from Steered Molecular Dynamics Simulations Using Jarzynski's Equality, J. Chem. Phys. 119 (2003) 3559–3566.
- [83] C. Jarzynski, Nonequilibrium Equality for Free Energy Differences, Phys. Rev. Lett. 78 (1997) 2690–2693.
- [84] J. Gore, F. Ritort, C. Bustamante, Bias and Error in Estimates of Equilibrium Free-Energy Differences from Nonequilibrium Measurements, Proc. Natl. Acad. Sci. U. S. A. 100 (2003) 12564–12569.
- [85] I. Kosztin, B. Barz, L. Janosi, Calculating Potentials of Mean Force and Diffusion Coefficients from Nonequilibrium Processes without Jarzynski's Equality, J. Chem. Phys. 124 (2006) 64106.
- [86] Q. Wei, W. Zhao, Y. Yang, B. Cui, Z. Xu, X. Yang, Method Evaluations for Adsorption Free Energy Calculations at the Solid/Water Interface through Metadynamics, Umbrella Sampling, and Jarzynski's Equality, ChemPhysChem 19 (2018) 690–702.
- [87] S. Wang, E. Zhu, Y. Huang, H. Heinz, Correlation of Oxygen Adsorption on Platinum-Electrolyte Interfaces with the Activity in the Oxygen Reduction Reaction, Sci. Adv., 7 (2021) eabb1435